NASA TECHNICAL MEMORANDUM

NASA TM X-53300

August 6, 1965

NASA TM X-53300

PEGASUS THERMAL DESIGN

by TOMMY C. BANNISTER
Research Projects Laboratory

NASA

George C. Marshall
Space Flight Center,
Huntsville, Alabama

NASA-GEORGE C. MARSHALL SPACE FLIGHT CENTER

TECHNICAL MEMORANDUM X-53300

August 6, 1965

PEGASUS THERMAL DESIGN

by

Tommy C. Bannister

SPACE THERMODYNAMICS BRANCH

RESEARCH PROJECTS LABORATORY

ACKNOWLEDGEMENT

The author is indebted to Mr. William C. Snoddy of MSFC and to Mr. Robert Eby of Fairchild-Hiller Corp. who contributed so much to the success of the Pegasus Thermal Design.

TECHNICAL MEMORANDUM X-53300

PEGASUS THERMAL DESIGN

by

Tommy C. Bannister

George C. Marshall Space Flight Center

Huntsville, Alabama

ABSTRACT

35103

Many of the components of the Pegasus spacecraft will function properly only so long as their temperatures are maintained within certain tolerances. The thermal requirements, thermal design, and orbital temperature results are presented in this report.

When the temperature specifications were received, two areas were recognized to be critical: (1) the micrometeoroid detector panels and (2) the electronics. This report deals primarily with these areas.

Quick-look results of the flight data from Pegasus A and B indicate that the thermal design was very successful. None of the component temperatures has extended beyond the design ranges. The critical batteries have been 300°K ± 6° K, which is well within their design range (270 °K to 322 °K), for over 150 orbits on Pegasus A.

author

TABLE OF CONTENTS

LIST OF ILLUSTRATIONS

TECHNICAL MEMORANDUM X-53300

PEGASUS THERMAL DESIGN

SUMMARY

Many of the components of the Pegasus spacecraft will function properly only so long as their temperatures are maintained within certain tolerances. The thermal requirements, thermal design, and orbital temperature results are presented in this report.

When the temperature specifications were received, two areas were recognized to be critical: (1) the micrometeoroid detector panels and (2) the electronics. This report deals primarily with these areas.

Quick-look results of the flight data from Pegasus A and B indicate that the thermal design was very successful. None of the component temperatures has extended beyond the design ranges. The critical batteries have been 300°K ± 6° K, which is well within their design range (270°K to 322 °K), for over 150 orbits on Pegasus A.

I. INTRODUCTION

The Pegasus satellite (Figure 1), formerly called the Micrometeoroid Measurement Capsule, was developed by the Fairchild-Hiller Corporation† under the supervision of the Marshall Space Flight Center, Huntsville, Alabama. Pegasus-A was injected into orbit on February 16, 1965 by SA-9; Pegasus B was orbited May 25, 1965 by SA-8; Pegasus C will be orbited later by SA-10. The primary mission of these spacecraft is the micrometeoroid measurement experiment designed to obtain statistical data on micrometeoroids. The satellite is required to have a large micrometeoroid detection area, a long lifetime (about 18 months), and a slowly changing random orientation in space. The planned orbital characteristics were a perigee of 486.9 km, an apogee of 747.7 km, and a period of 97.14 minutes. The actual elements of Pegasus-A were 496.4 km perigee, 743.5-km apogee, and a 97.10-minute period. Initially, Pegasus-A was spinning about its longitudinal axis (X-axis). Since the X-axis is not the principle moment of inertia, the satellite began to precess, with the angle of precession gradually increasing until the only mode of spin became the mode about the principle moment of inertia (the y-axis, which is normal to the detector surface). This transition was completed within approximately eight days after launch on Pegasus A.

The initial task in the thermal design was to obtain the thermal specifications of the various components of the spacecraft, and to become familiar with the mission and hardware thermal requirements so that the

† Formerly Fairchild-Stratos Corporation

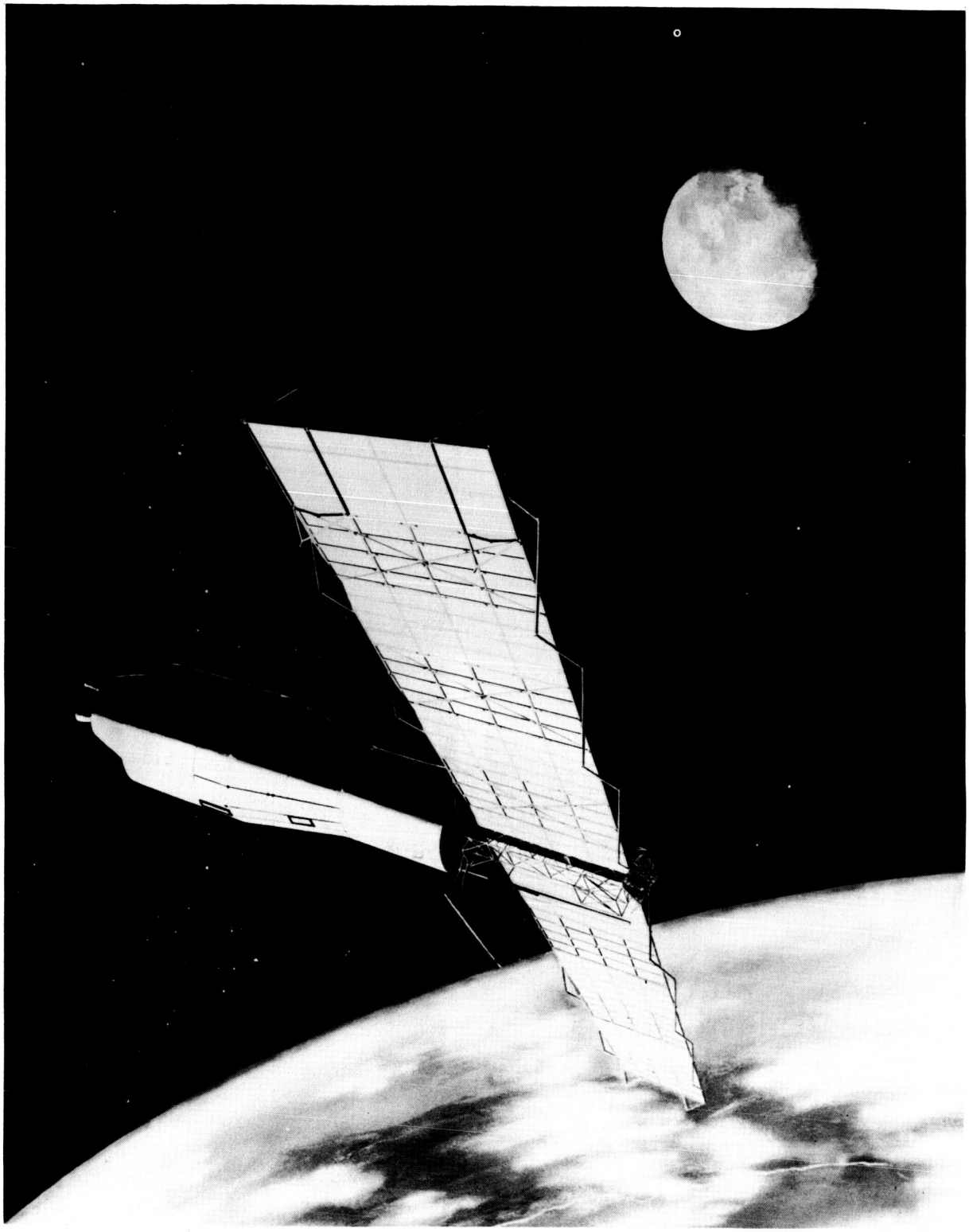

FIGURE 1 THE PEGASUS SATELLITE

thermal design concepts and criteria could be formulated which would not interfere unnecessarily with the other design areas.

The micrometeoroid detector panels and the electronics were the critical areas for thermal design. The problem associated with the detector panels was the possibility of severe thermal variations which could conceivably cause panel delamination. A detailed study of this problem revealed that the only readily controllable parameters were the optical properties of the panel exterior surfaces. The orbital temperatures were defined for all sets of possible optical properties. A search was made to find the coating with suitable optical properties; the chemical conversion coating, Alodine, was finally selected. This coating was subjected to ultraviolet radiation (Figure 2) in the laboratory to verify the space stability of its properties. Also, a detector panel was studied in a thermal-space chamber at hard vacuum.

The thermal problem associated with the electronics is ensuring that they do not go beyond the prescribed "upper" and "lower" limits. The temperatures of most electronic components is a strong function of internal heating rates, thermal linkage to the supporting structures, structure temperature, and radiation heat transfer to other parts of the spacecraft and to space. Usually, several of these can be controlled to a degree by design. Where possible, the electronic components were placed in a thermally insulated canister (Figure 3) with a "sized window" to radiate the internally generated heat to a cold sink. This window was faced toward the vehicle to eliminate direct solar radiation from entering the canister. With random orientation, such a variable input as the direct solar radiation would greatly increase the design requirements.

Throughout this report the terms "SMA" and "sink" are used

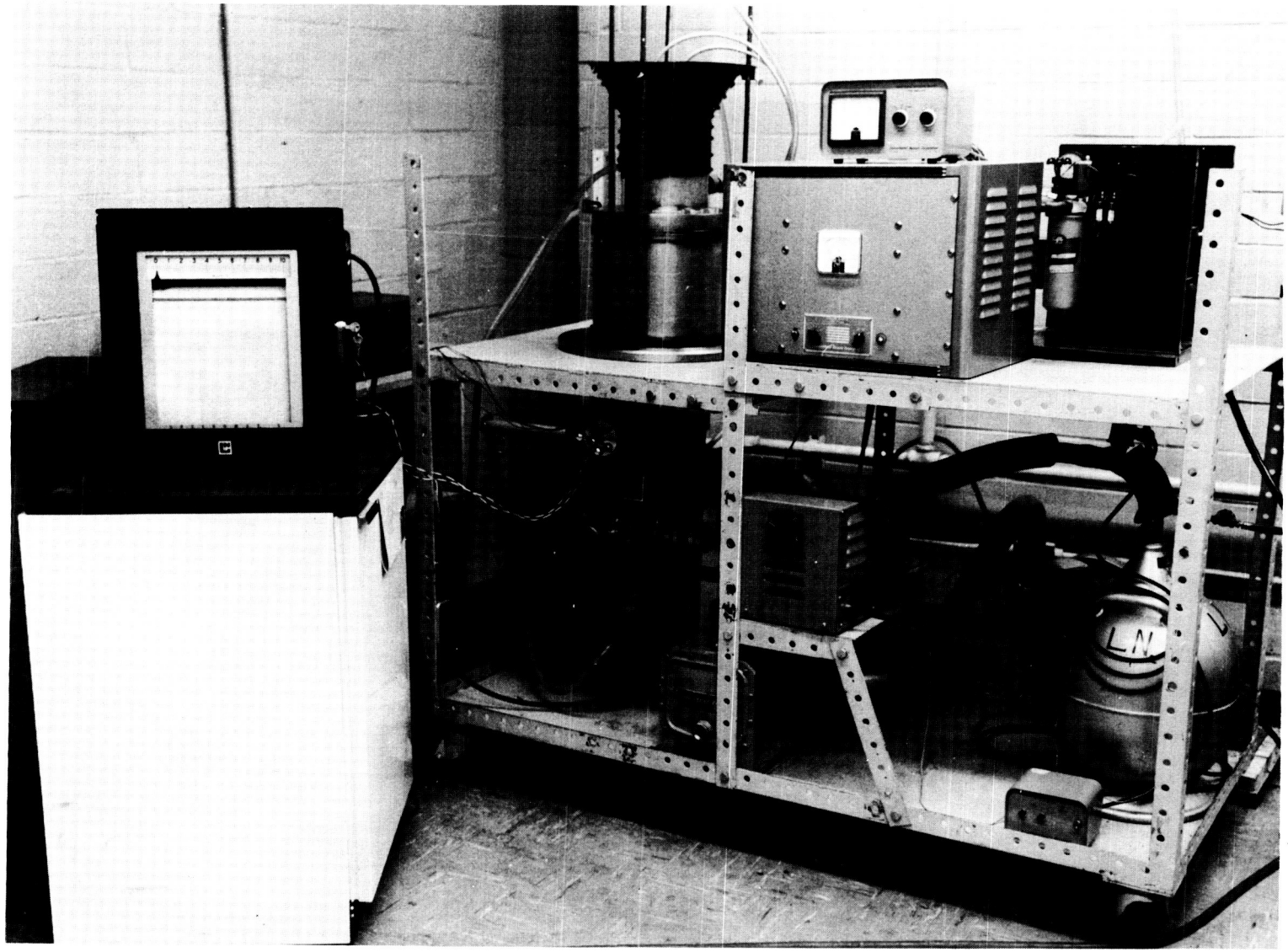

FIGURE 2 ULTRAVIOLET IRRADIATION FACILITY

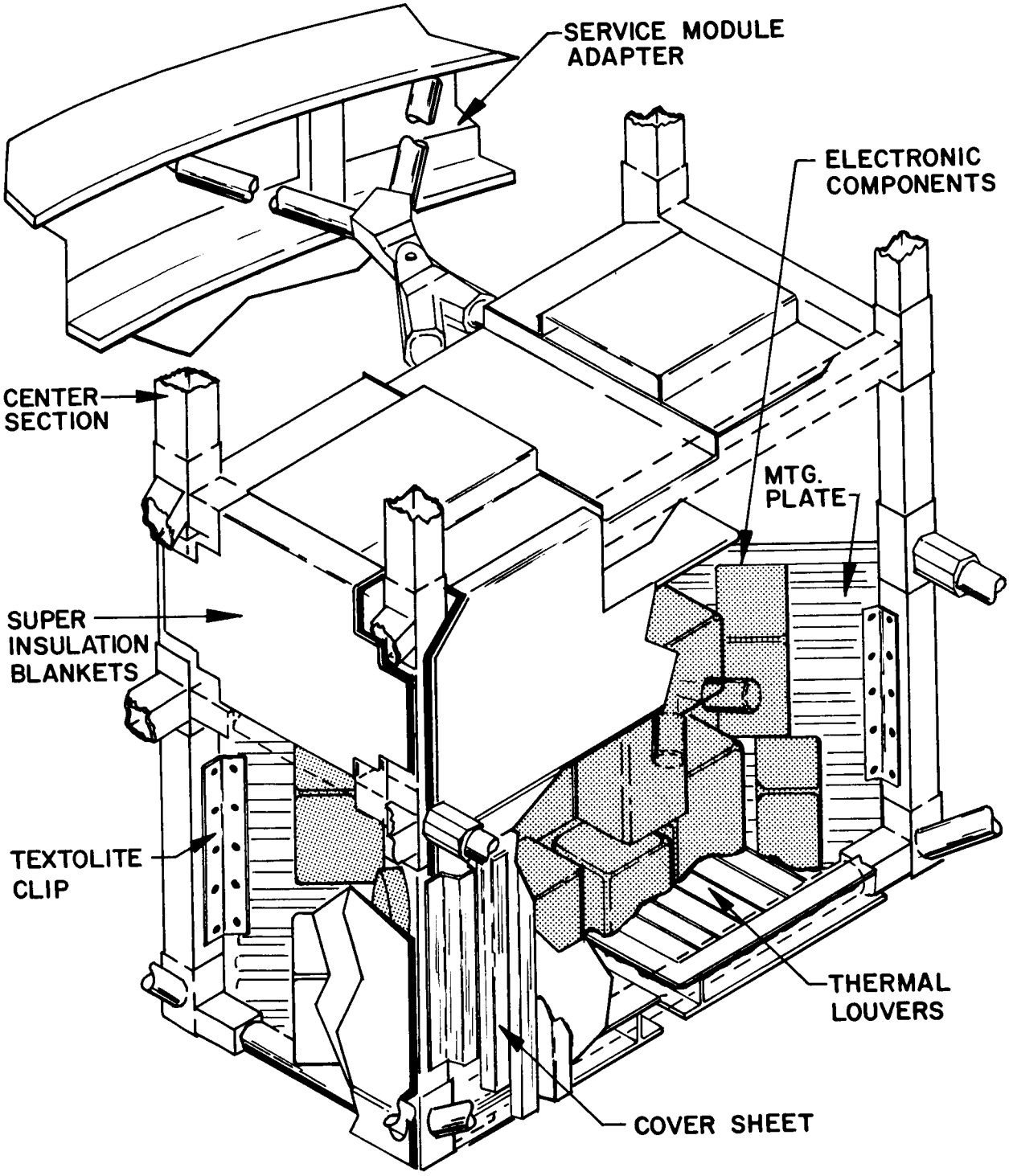

FIGURE 3 THE ELECTRONICS CANISTER

interchangeably when speaking of the canister radiation heat sink. This SMA is an adaptor to the Service Module. The window sees the internal areas of the SMA, IU (Instrument Unit), and S-IV stage bulkhead (Figure 4).

Since most of the factors affecting the canister thermal design are variable, it is useful to consider a thermodynamic "hot" and a thermodynamic "cold" case. If the varying factors are not too severe, the window could be sized to keep both the hot and cold cases within specified limits.

With moderate parameter variations, the steady-state "hot" and "cold" extreme temperatures can each be kept within the design range. In the case of Pegasus, it became apparent that this was an inadequate method of control. After several alternatives were evaluated, an active louver system (Figure 5) was employed which prohibits radiant heat flow through the window in the cold case without much hindrance to the heat flow in the hot case.

II. THERMAL REQUIREMENTS OF PEGASUS IN ORBIT

A list of thermal specifications for the components of Pegasus was prepared by the contractor. A summary outline of the thermal requirements is as follows:

A. ELECTRICAL COMPONENTS

1. Inside the Canister

a. Batteries	272°K to 322°K
b. Others	262°K to 332°K

2. Outside the Canister

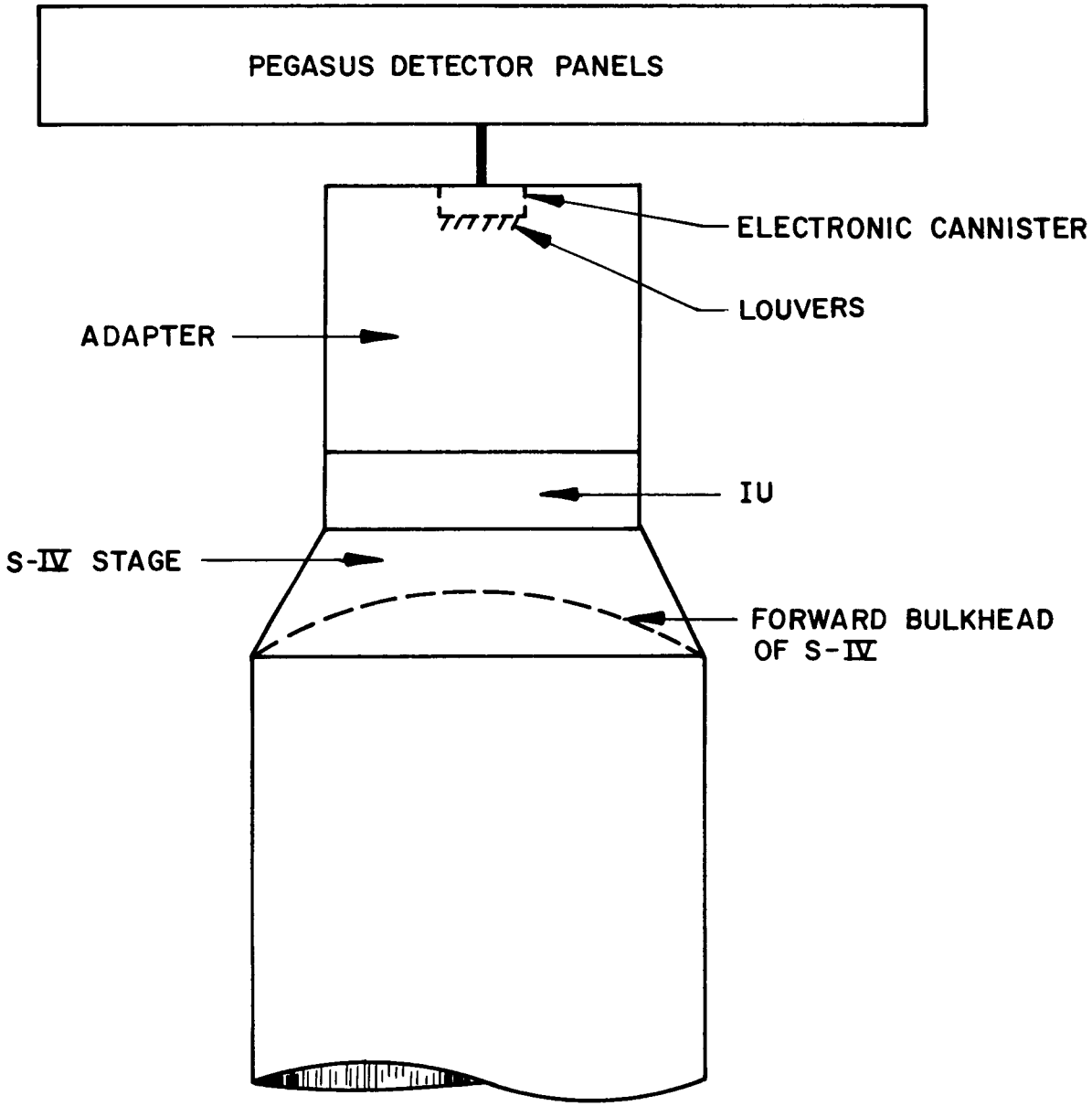

FIGURE 4 THE OPEN END OF THE VEHICLE AS A TEMPERATURE SINK

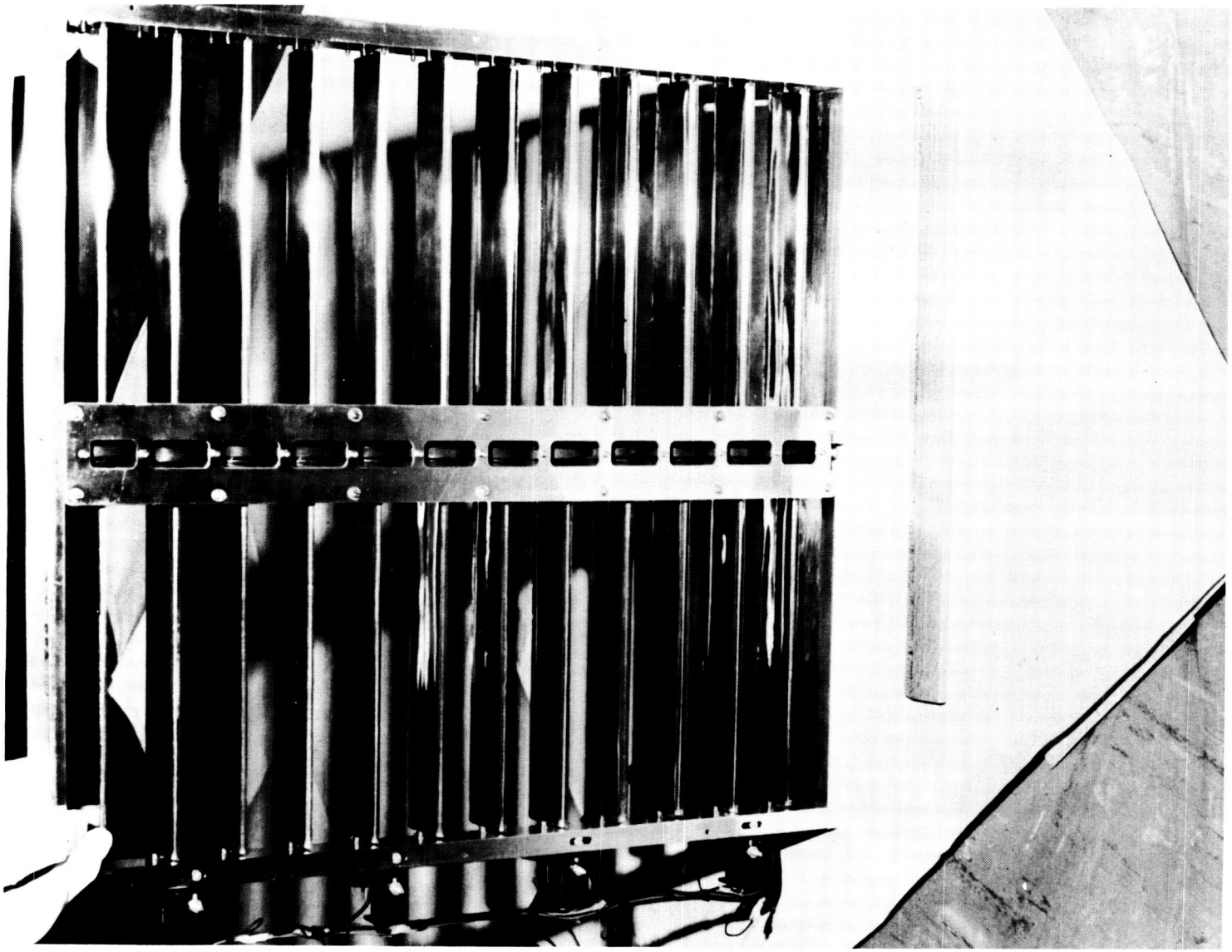

FIGURE 5 THE THERMAL CONTROL LOUVERS

	a. Zener diodes	218°K to 358°K
	b. Solar cells	222°K to 388°K
B.	OTHER COMPONENTS	
	1. Micrometeoroid detector panels	167 K to 394 K and $\dot{T}$ less than 100 K/min.
	2. Infrared sensors	218 K to 358 K
	3. Radiation detector	222 K to 388 K

III. THERMAL DESIGN

A. ANALYSIS

1. Thermal Design of the Electronic Canister. The analysis of the electronic canister consisted of two parts: (1) desk calculations of representative average heat balance equations, and (2) detailed studies performed utilizing a complex computer program. The computer studies were used to validate the desk calculations.

The canister (Figure 3) was designed to be thermally isolated for the following reasons: (1) to prevent the components from being thermally linked to heat sources of difficult-to-determine temperatures, such as the Pegasus center structure; (2) to insure that the components will not be affected by varying radiant sources of heat, such as direct solar radiation; and (3) by minimizing extraneous heat transfer, the "controllable" heat transfer is maximized. Therefore, the difference in "controllable" heat transfer between the "hot" and "cold" cases is minimized. This is most important because it is basically this difference that determines the amount of active thermal control required. (With zero difference, the area of the open face could be simply "sized" to give the proper temperature, or with a very large difference, louvers would not accomplish thermal

control.)

Primarily three techniques were employed to obtain this thermal isolation: (1) The canister side walls were equipped with ten layers of super-insulation,† consisting of highly reflective sheets of aluminized Mylar which greatly restrict radiant heat transfer through the side walls; (2) The internal mounting bracket for the components was fashioned as a double "y" and attached to the supporting structure with special fiber-glass chips to restrict heat conduction to the center-structure; (3) The connecting cables and possible radiant heat leakage areas were covered with a low-emittance aluminized Mylar tape, which minimized the radiant linkage between the canister components and certain cold structures.

2. The Average Heat Balance Analysis. In systems with large thermal time constants, the average heat balance analysis can usually be used without difficulty. Care must be given to ensure that erroneous results are not obtained in an oversimplified model. The analysis employed in the thermal design of the Pegasus electronics canister was carefully worked out, and later verified by more detailed computer studies and thermal vacuum tests.

Two of the dominant heat inputs vary primarily because of eclipse of the sun by the earth. It is useful, therefore, to define T_x as the percentage of time-in-sunlight per orbit. For the Pegasus orbit, the range of T_x is 63% to 78%.‡ The internal heat generation of the electronics depends upon T_x primarily because the solar cell output

†Mr. Jack Light at National Research Corporation was employed as advisor in the use of superinsulation.

‡"Calculations Concerning the Passage of a Satellite Through the Earth's Shadow" Marshall Space Flight Center Report, MTP-RP-61-1, Feb. 1961, by William C. Snoddy.

depends on the amount of incident sunlight. Also, the solar radiation absorbed by the external satellite surfaces depend strongly on T_x.

The prelaunch internal heat generation was determined by Mr. Mott of Fairchild-Hiller Corporation to be 45W to 63W, when averaged over one orbital period.

The T_x is also used, together with the following attitude considerations, to determine the sink temperature as a function of the radiometric, or optical properties of the SMA, IU, and S-IV external surfaces.

Perhaps the most important consideration in the thermal design of Pegasus canister is solar attitude. Obviously, if the long cylindrical SMA, IU, and S-IV become oriented with the rear of the S-IV toward the sun, the sink temperatures (T_s) will become very cold. If this never occurs for any appreciable length of time, then the range of T_s is substantially reduced. A special "thermal factor" was calculated by Mr. Robert Holland of MSFC, who performed the prelaunch attitude analysis of the Pegasus. This factor represents the average projected area of the sink over various time periods. This factor was calculated for the many possible orbital situations. Therefore,

$$\Upsilon = \frac{1}{t} \int_0^t \sin \theta \, d\, t \quad \lim_{t \to \infty} \Upsilon = 2/\pi$$

where

θ = sun angle of the longitudinal axis of the S-IV

t = time

Υ = thermal factor

In all attitude cases considered, Υ was never less than 0.6 for t within the thermal time constant indicating that the tumble period was always less than the thermal time constant (15 hours). For Pegasus,

this is of tremendous consequence, because the range of T_s would otherwise be about three times the present value, and the present thermal design would be inadequate. Analytically, this will mean that the average projected area to the sun (needed in evaluating the T_s) can be used for a rapidly tumbling cylinder.

Now to evaluate the temperatures analytically, the heat-balance equation for the sink is given:

$$\frac{1}{\tau} \int_{o}^{\tau} \sum_{i=1}^{N} \dot{Q}_i \, dt = 0 \ ,$$

where $\dot{Q}_i$ = heat flow rates into the sink

dt = differential time

τ = orbital period

Expanding and separating, the following form can be obtained for T_s:

$$\left(\frac{T_s}{100}\right)^4 = \frac{S}{\sigma\pi} \left\{ {}^{\alpha_s}/_{\epsilon_T} \left[\cos (MAS)\, T_x + \frac{F_{\gamma r}\, \overline{\cos(RAS)}}{2} \right] + F_{\gamma r}\, E \right\} + \frac{\dot{Q}_o}{\sigma A_T} \ ,$$

where $\dot{Q}_o$ = flux through the top of the SMA

A_T = external area of the SMA, IU, and S-IV

Other parameters are defined in Table I.

Table II lists the various combinations of values which were evaluated and used to generate T_s (Figure 6).

The canister temperature (T_c) is now expressed in terms of T_s with its heat-balance relation:

$$A\, F \sigma \left[\left(\frac{T_s}{100}\right)^4 - \left(\frac{T_c}{100}\right)^4 \right] + \dot{Q}_l + \dot{Q}_g = 0 \ ,$$

TABLE I

Symbol	Parameter	Units
σ	Stefan-Boltzmann constant	watts/m^2 $^\circ K^4$
α_s	Solar absorptance	--
ϵ_{IR}	Infrared Emittance	--
MAS	Solar-satellite angle	--
RAS	Solar-satellite radius angle	--
RAM	Satellite-satellite radius angle	--
S	Solar constant	watts/m^2
B	Albedo constant	"
E	Earth's IR constant	"
$F_{\gamma r}$	Earth Radiation Geometry Factor	--
P	Orbit period	sec
T_x	% time in sunlight	--
T_i	Temperature of node i	$^\circ K$
$\dot{T}_i$	Time rate of change of Ti	$^\circ K$/sec
$\dot{Q}_i$	A heat flux	watts
F	Emissivity factor	--
H_i	Heat capacity	Joules/$^\circ K$
R_{ij}	Radiance	watts/$^\circ K^4$
C_{ij}	Conductance	watts/$^\circ K$

TABLE II

Case I (Broadside tumble)

(1) Tx = .78
(2) F_{γ_r} = .5
(3) cos $(MAS)_1$ = 1
(4) no flux thru open end

Case II (Broadside tumble)

(1) Tx = .78
(2) F_{γ_r} = .5
(3) cos $(MAS)_1$ = 1
(4) open end has $\alpha_s = \epsilon_{IR} = .9$

Case III (In plane tumble)

(1) Tx = .78
(2) F_{γ_r} = .5
(3) cos $(MAS)_1$ = .637
(4) open end has $\alpha_s = \epsilon_{IR} = .9$

Case IV (In plane tumble)

(1) Tx = .78
(2) F_{γ_r} = .5
(3) cos $(MAS)_1$ = .637
(4) no flux thru open end

Case V (Broadside tumble)

(1) Tx = .63
(2) F_{γ_r} = .25
(3) cos $(MAS)_1$ = 1
(4) open end has $\alpha_s = \epsilon_{IR} = .9$

Case VI (Broadside tumble)

(1) Tx = .63
(2) F_{γ_r} = .25
(3) cos $(MAS)_1$ = 1
(4) no flux thru open end

Case VII (In plane tumble)

(1) Tx = .63
(2) F_{γ_r} = .25
(3) cos $(MAS)_1$ = .637
(4) open end has $\alpha_s = \epsilon_{IR} = .9$

Case VIII (In plane tumble)

(1) Tx = .63
(2) F_{γ_r} = .25
(3) cos $(MAS)_1$ = .637
(4) no flux thru open end

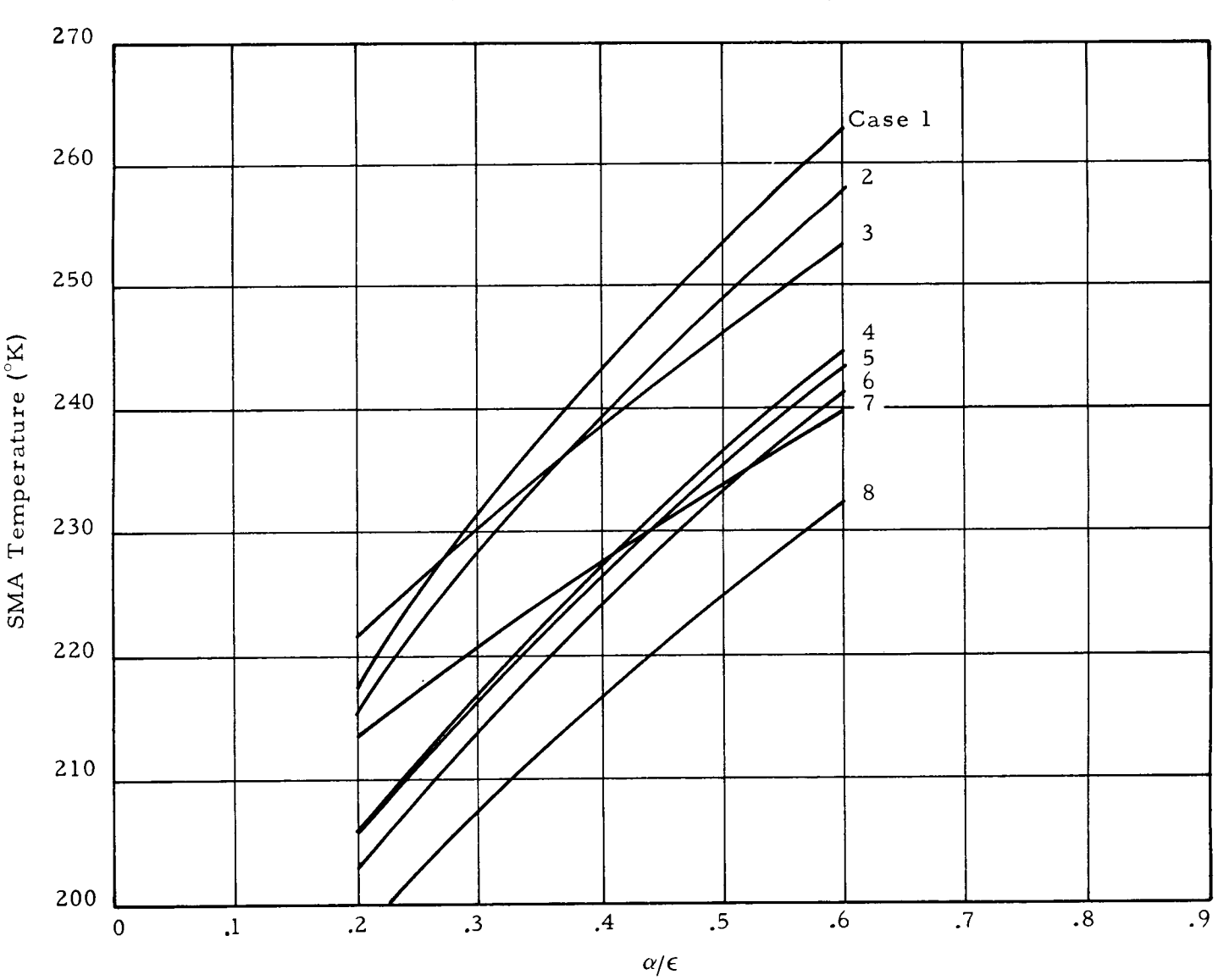

FIGURE 6 - THE ORBITAL SINK TEMPERATURES

where $\dot{Q}_g$ = average orbital internal heat generation of the canister

$\dot{Q}_l$ = extraneous heat loss through insulation, etc.

A = area of radiating window

F = radiation factor

As expected, parametric studies revealed that the mean value of T_s, range of T_s, and value of $\dot{Q}_l$ were of prime importance. $\dot{Q}_l$ has to be minimized; the range of T_s must be minimized; and T_s must be cold in order to obtain the greatest effect of the window for control. Thus, a low α_s/ϵ_T space stable coating was desired. After an exhaustive search, S-13† (ZnO in Methyl Silicone) was recommended by Mr. Edgar R. Miller of MSFC. After due consideration of the laboratory data available, a range of 0.2 to 0.3 of α_s/ϵ_T was established to be used in the thermal design calculations of T_s. The $\dot{Q}_l$ range was calculated to be approximately 10W to 40W. An "A" could not be selected which would maintain T_c within its limits. This means that the compensation obtained by $(T_s^4 - T_c^4)$ was not sufficient between the hot and cold case. After a comprehensive study, thermal control louvers similar to those used on Mariner II were added to the canister window in order to make F controllable ($.15 < F < .60$).‡ (It is noted that with louvers, one must replace $(T_s^4 - T_c^4)$ with $(T_e^4 - T_c^4)$ where $T_e^4 = \frac{T_s^4 + T_c^4}{2}$ when the louvers are closed.) The range of the canister temperature is then $275^\circ K$ to $305^\circ K$.

† The S-13 is a highly reflective white paint developed at the Illinois Institute of Technology (IIT) under sponsorship of MSFC. This coating was shown to be space stable ($\Delta\alpha_s \cong 0.04$) after 200 hours of 10 sun-intensity ultraviolet irradiation at IIT.

‡ Plamondon, Joseph A., Analysis of Movable Louvers for Temperature Control, Jet Propulsion Lab., Rpt. TR 32-555, Pasadena, California, January 1964.

3. Computer Analysis of the Electronics Canister. This analysis evaluated the calorimetric heat-balance equations without resorting to the use of averaging, etc.; the thermodynamic model broken down into 45 nodes with 45 simultaneous first-order differential equations. These equations are solved on the IBM 7090 Mod. II, utilizing the "General Space Thermal Program" developed at Marshall by W. C. Snoddy and T. C. Bannister, Appendix I, Article I and III. The sink temperature range obtained was 209°K to 240°K. Several runs were made using various values of the parameters directly affecting the canister temperatures. The results were very similar to those obtained by the average heat-balance calculations.

4. The Thermal Analysis of the Micrometeoroid Detector Panels. Unlike the electronics canister, the detector panels (Figure 7) possessed a very small time constant (on the order of ten minutes). This caused rapid thermal fluctuations of the panel temperatures as the satellite travelled in and out of the earth's shadow at various solar angles. Hand calculations are impractical in an analysis where high rates of change are to be considered, so the computer was used exclusively for defining the temperature excursions in orbit for the detector panels. The computer analysis is based on a 4-node thermal model having the following characteristics:

(1) The panel is an infinite slab of foam 2.54 cm thick (one-dimensional heat flow analysis)

(2) Foam density - 480 Kg/m^2

(3) The specific heat - 1350.0 Joules/$Kg^{\circ}K$

(4) The foam thermal conductivity - 0.015 watts/$m^{\circ}K$ at 200°K
0.041 watts/$m^{\circ}K$ at 300°K
0.137 watts/$m^{\circ}K$ at 400°K

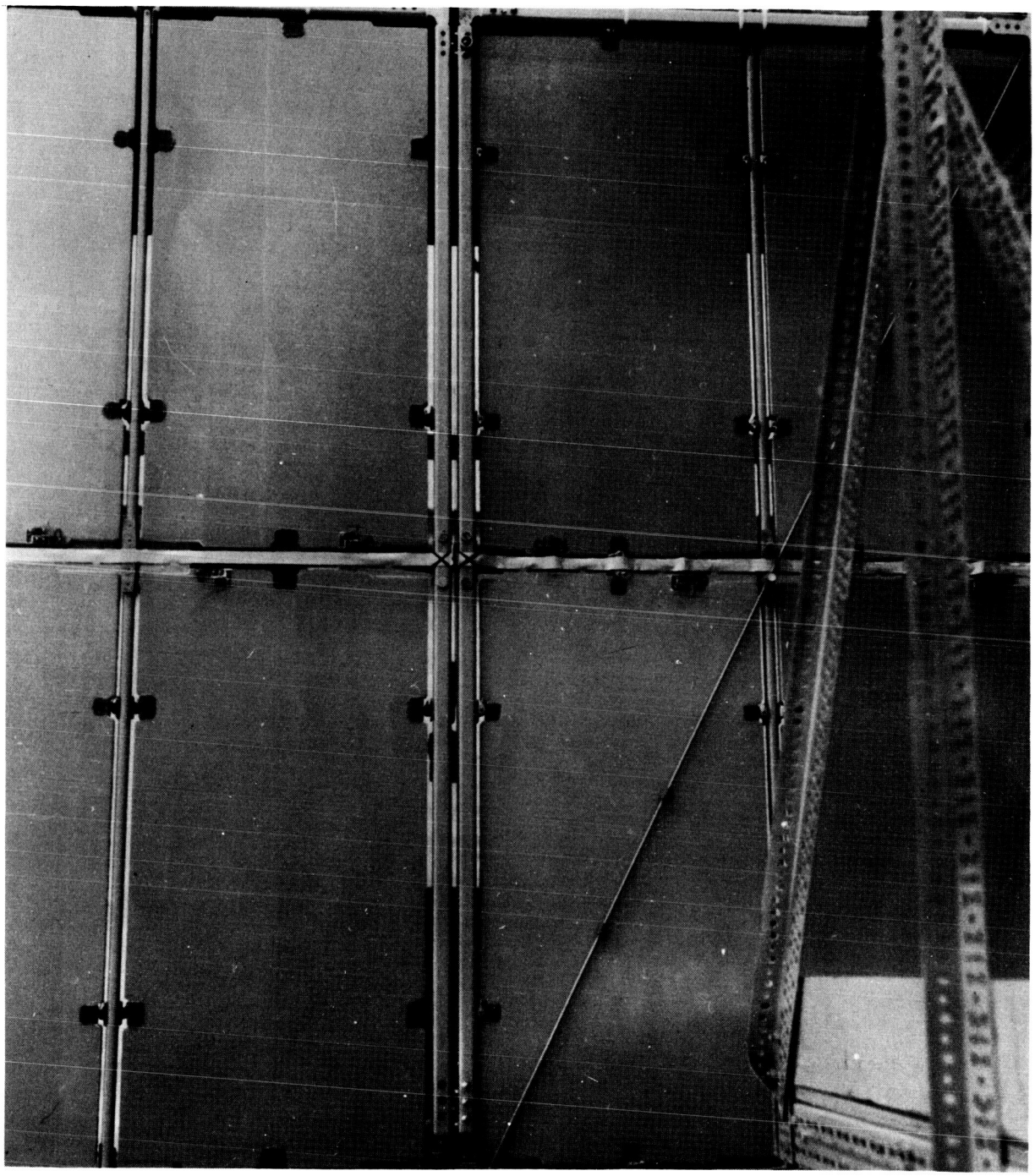

FIGURE 7 THE MICROMETEOROID DETECTOR PANELS

(5) The slab is considered to have four equal layers of material. (The heat capacity of the aluminum target sheets is included in the outside layers.)

(6) α_s and ϵ_T are floating parameters

This model is adapted to the "General Space Thermal Program" (Article 1 and II, Appendix I) from which typical curves as shown in Figures 8 thru 11 were obtained. Figures 8 and 11 represent the solar broadside and solar null cases which are extreme cases.

Examination of the results showed that a low α_s / ϵ_T minimizes the maximum temperature and a low ϵ_T maximizes the minimum temperature. The limiting values required to keep the temperatures within the design limits were $\alpha_s / \epsilon_T \leq 1$ and $\epsilon_T \leq .6$. A space-stable chemical conversion coating, Alodine, was found which exhibited properties consistent with these specifications, and which was relatively inexpensive (compared to vacuum deposition of SiO on approximately 200 M^2 of detector surface). Nominal values of α_s / ϵ_T were .5/.6. A few panels had α_s / ϵ_T from .4/.6 to .5/.5.

5. Other Thermal Analysis. The IR sensors, zener diodes outside the electronic canister radiation detector, and solar cells were not analyzed in great detail. The analysis of Fairchild-Hiller Corporation was carefully evaluated and accepted.

B. LABORATORY STUDIES AND TEST

1. Detector Panel Laboratory Studies. Computer calculations have shown the detector panel orbital temperatures to be critical with respect to specifications for the case in which the panel is oriented broadside to the sun. This study was designed to simulate this condition as nearly as possible with the present laboratory techniques.

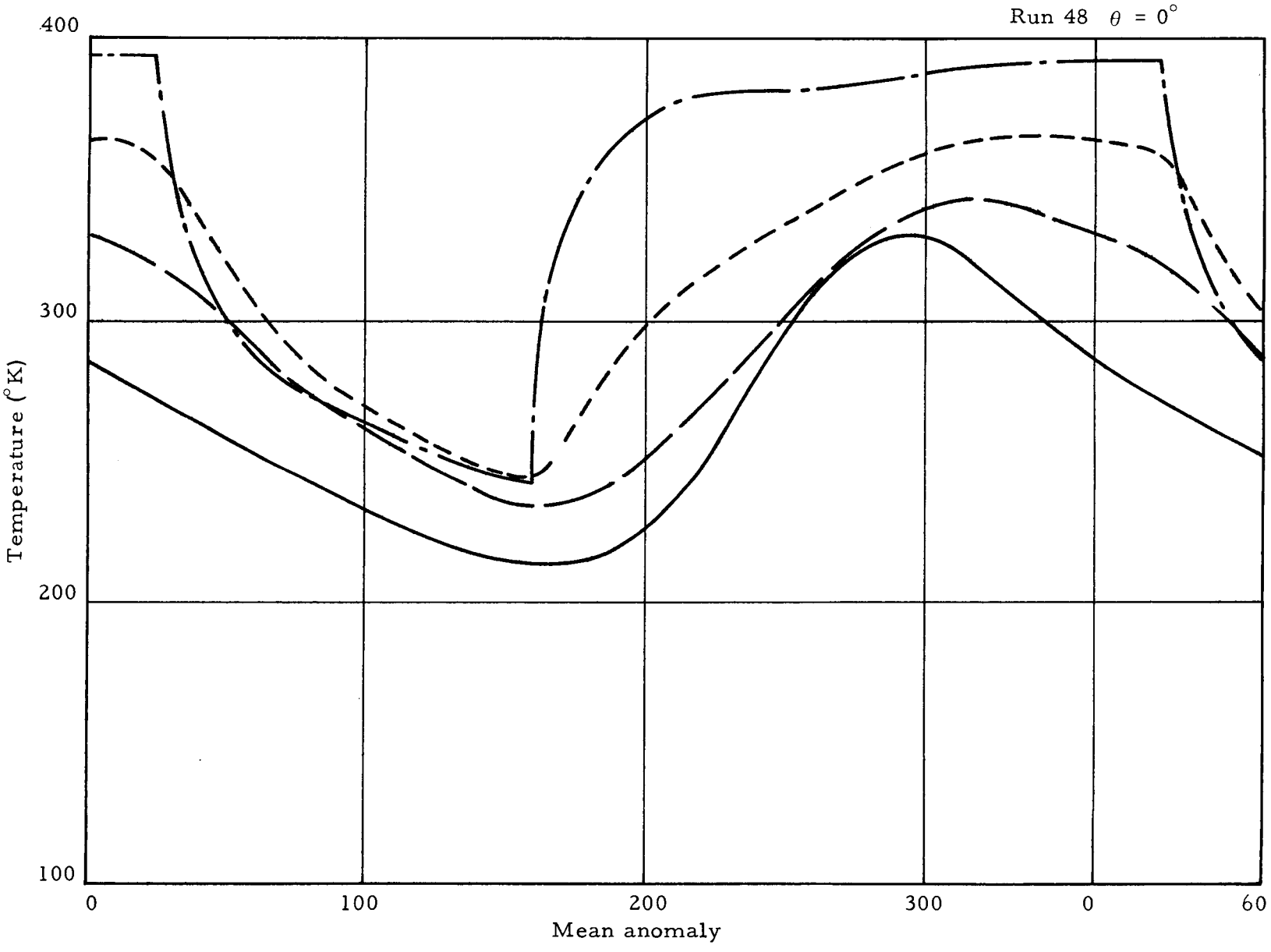

FIGURE 8 - CALCULATED DETECTOR PANEL TEMPERATURE (MAS = 0)

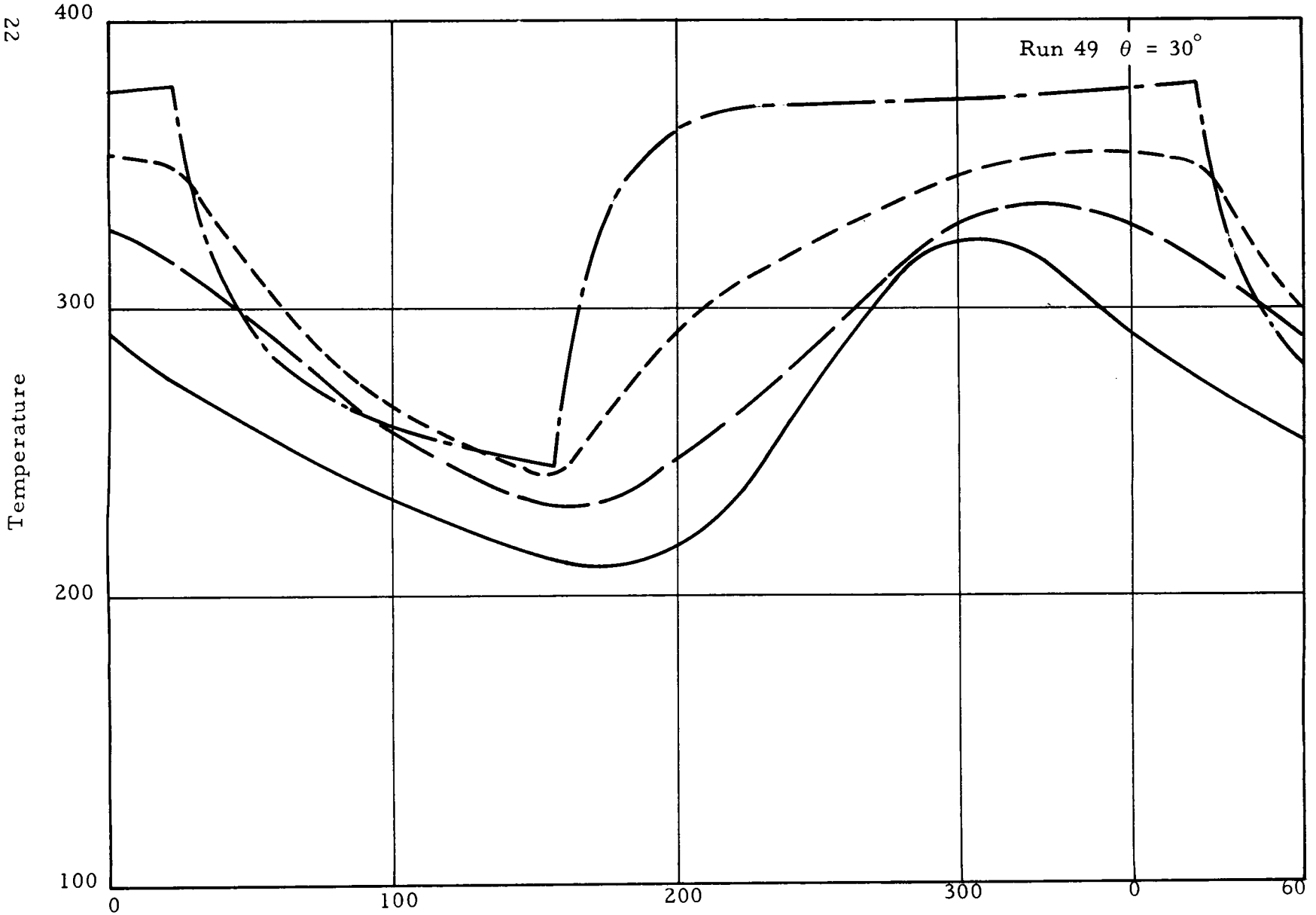

FIGURE 9 - CALCULATED DETECTOR PANEL TEMPERATURE (MAS = 30)

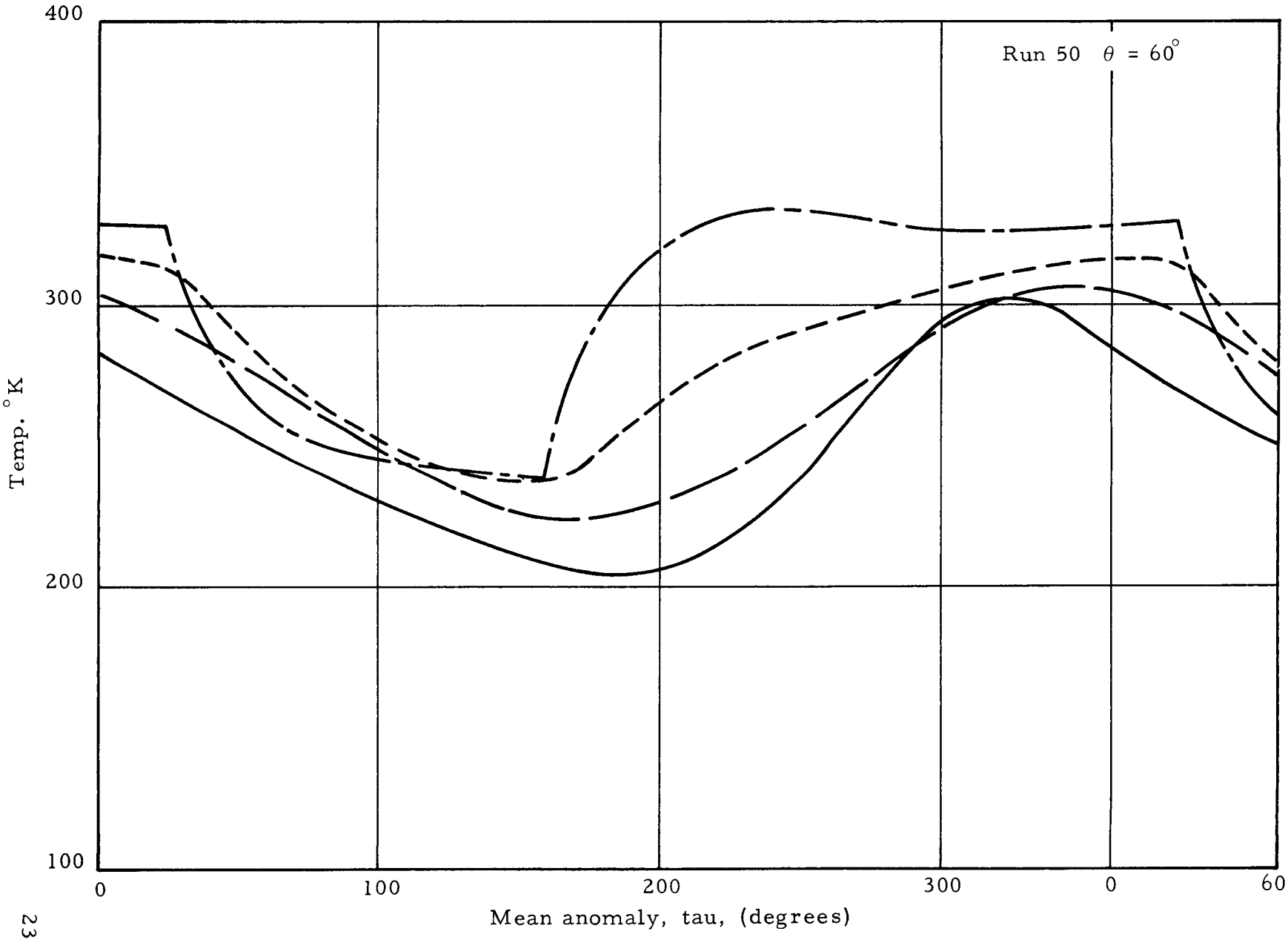

FIGURE 10 - CALCULATED DETECTOR PANEL TEMPERATURE (MAS = 60)

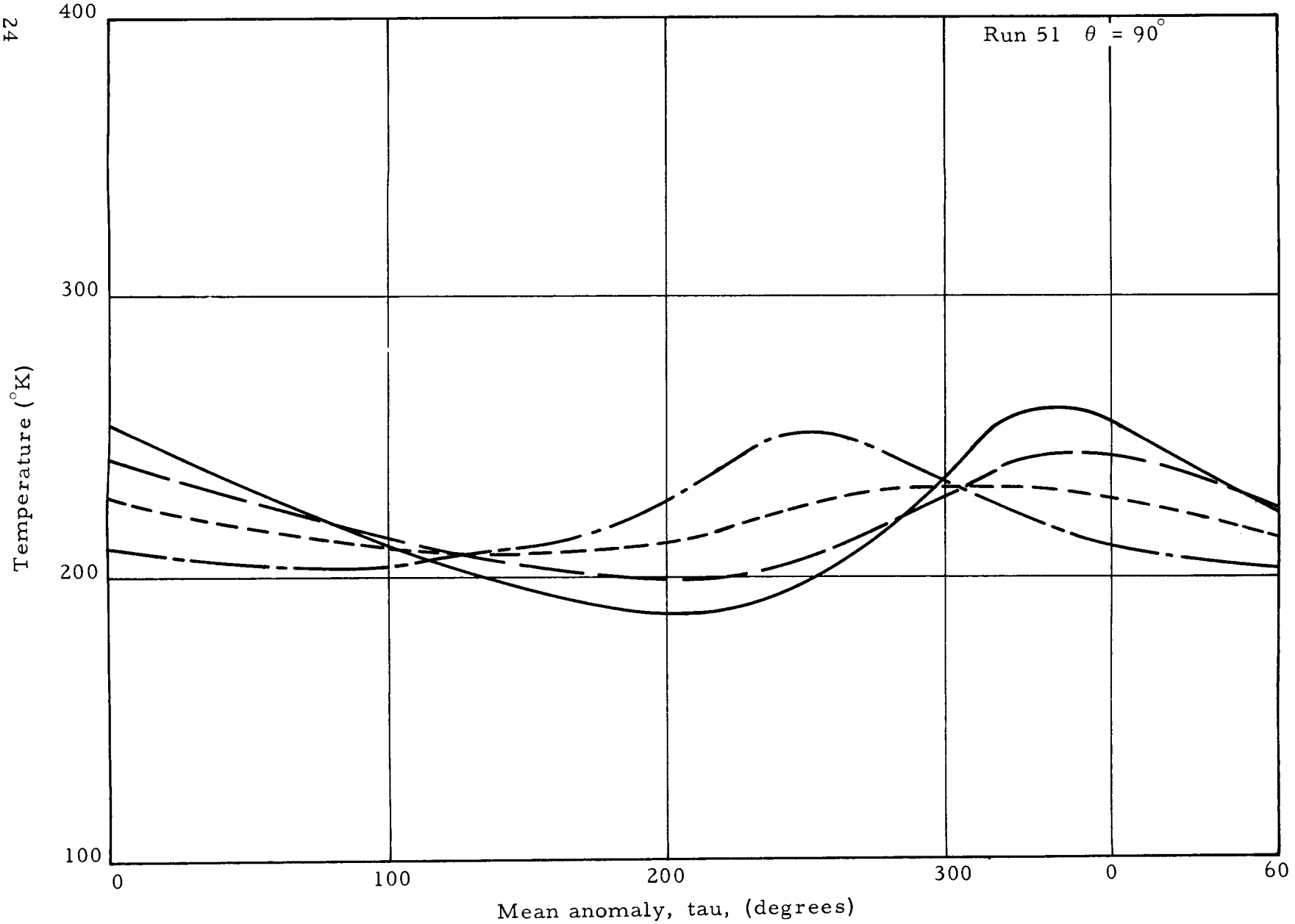

FIGURE 11 - CALCULATED DETECTOR PANEL TEMPERATURE (MAS = 90)

A 1-ft^2 detector panel was specially fabricated for this study by Schjeldahl. Eight thermocouples were embedded inside the panel during fabrication in two stacks of four each. The panel was situated in the thermal space chamber (Figure 12) Space Thermodynamics Branch (R-RP-T) of Research Projects Laboratory. (The panel faced a quartz window through which it was illuminated with a carbon arc lamp.) The lamp was switched on and off to simulate the shadow-sun condition of space. The intensity of the lamp was measured periodically with an Epply thermopile mounted on a rotary feedthrough. The chamber shroud was maintained at 77°K with LN_2, and the pressure fluctuated in the 10^{-6} to 10^{-7} torr range. Radiometric measurements were made on the Alodine surface at the thermocouple stacks prior to vacuum.

Figure 13 shows the measured temperatures for several runs. The maximum design limit of 398°K (250°F) was exceeded because the lamp intensity was greater than one sun. Calculations show remarkable agreement with theoretical results. A computer program was written for a detailed study and Fig. 14 shows the calculated temperature superimposed on the measured values. This study verified the thermodynamic model and the various thermophysical properties used in the thermal analysis of the detector panels.

2. Electronic Canister Thermal Vacuum Studies at Fairchild-Hiller Corp. A series of thermal vacuum studies made at Fairchild-Hiller Corporation (FHC), Bladensburg, Md., were closely monitored by the Space Thermal Branch of Research Projects Laboratory where the thermal design was verified and developed. The tests were designed to thermally simulate the SMA, S-IV, and Pegasus center structure temperatures, and to evaluate the resultant canister temperatures for both the "hot" and "cold" situations.

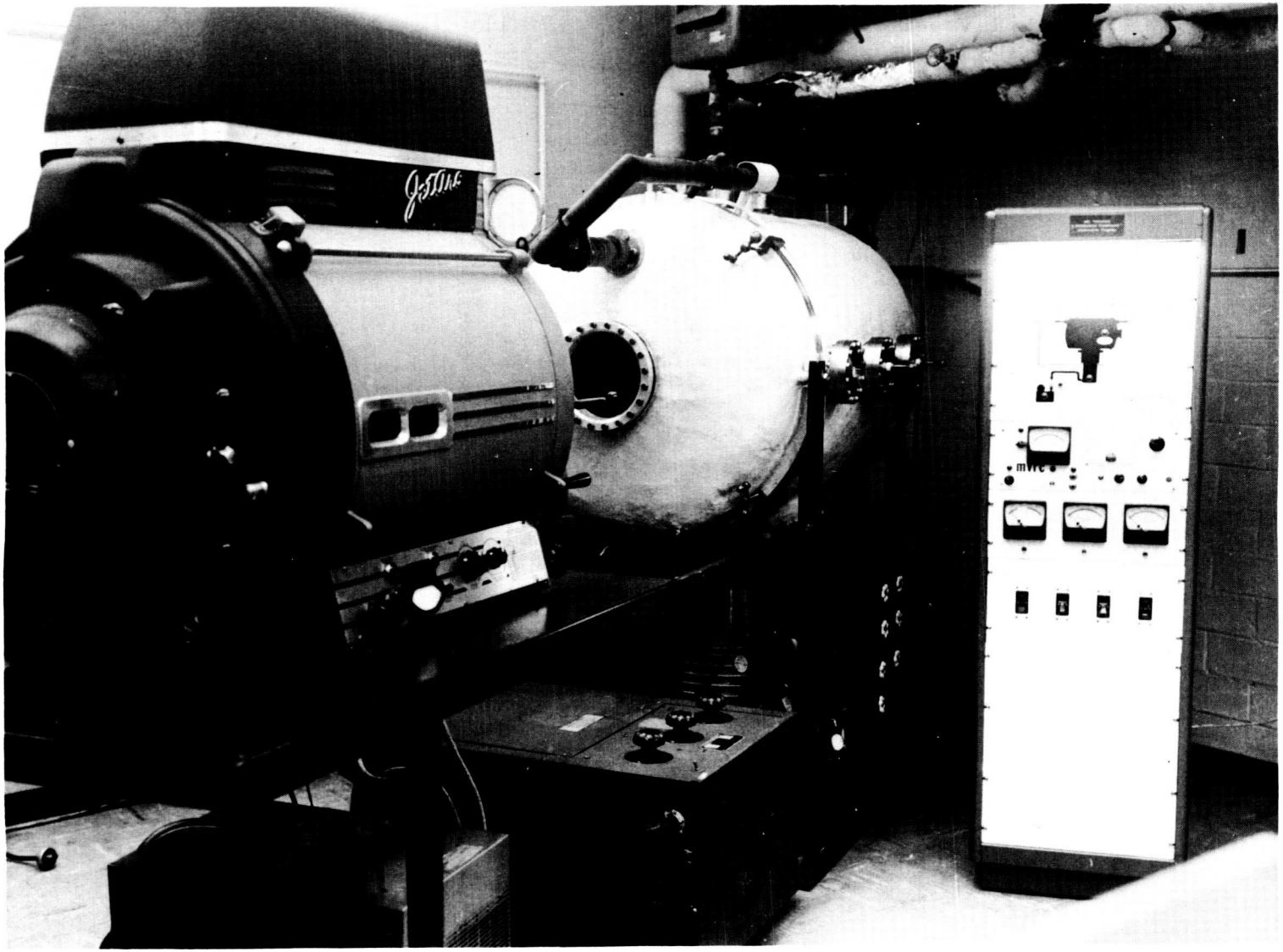

FIGURE 12 THE THERMAL SPACE CHAMBER

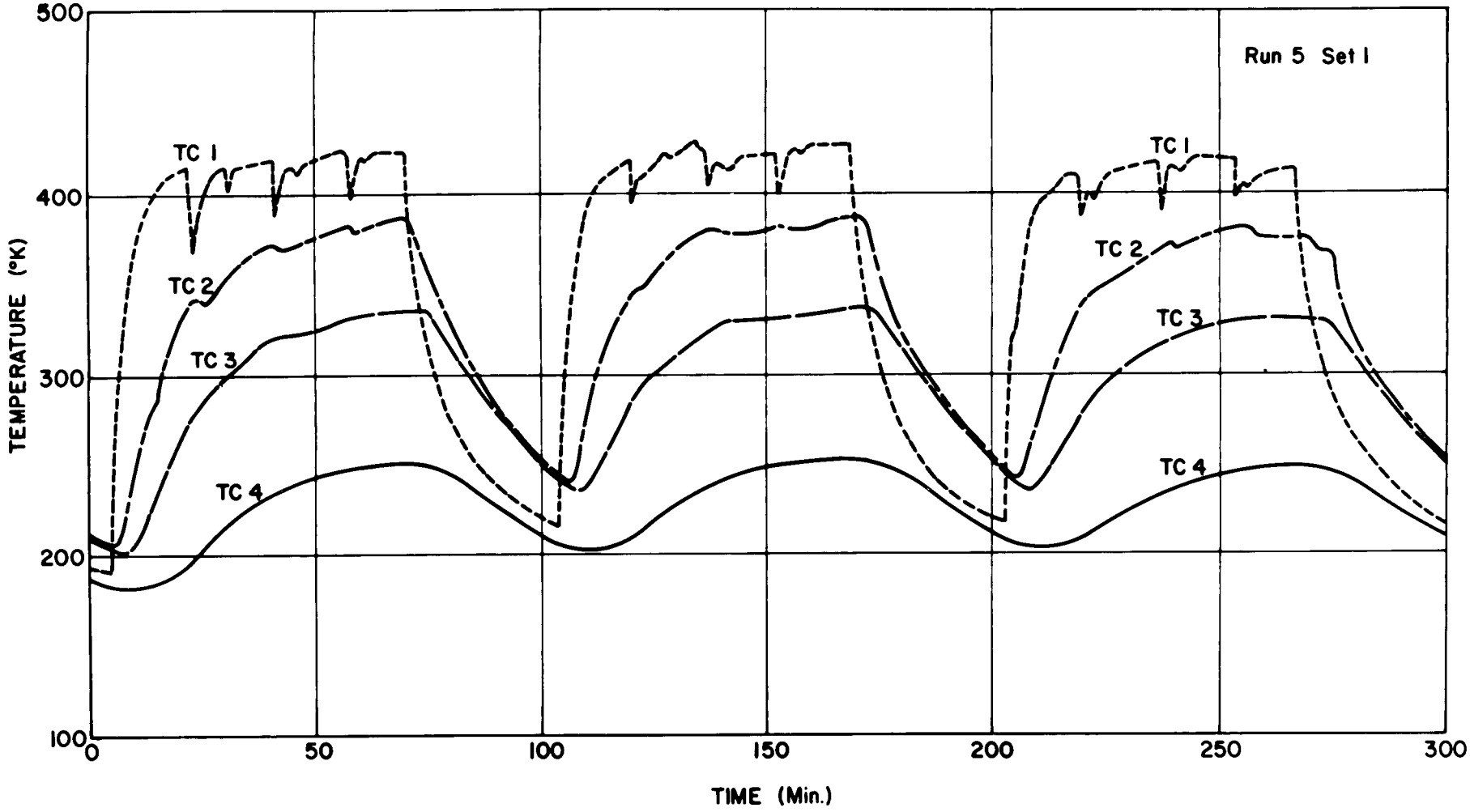

FIGURE 13 MEASURED DETECTOR PANEL TEMPERATURES

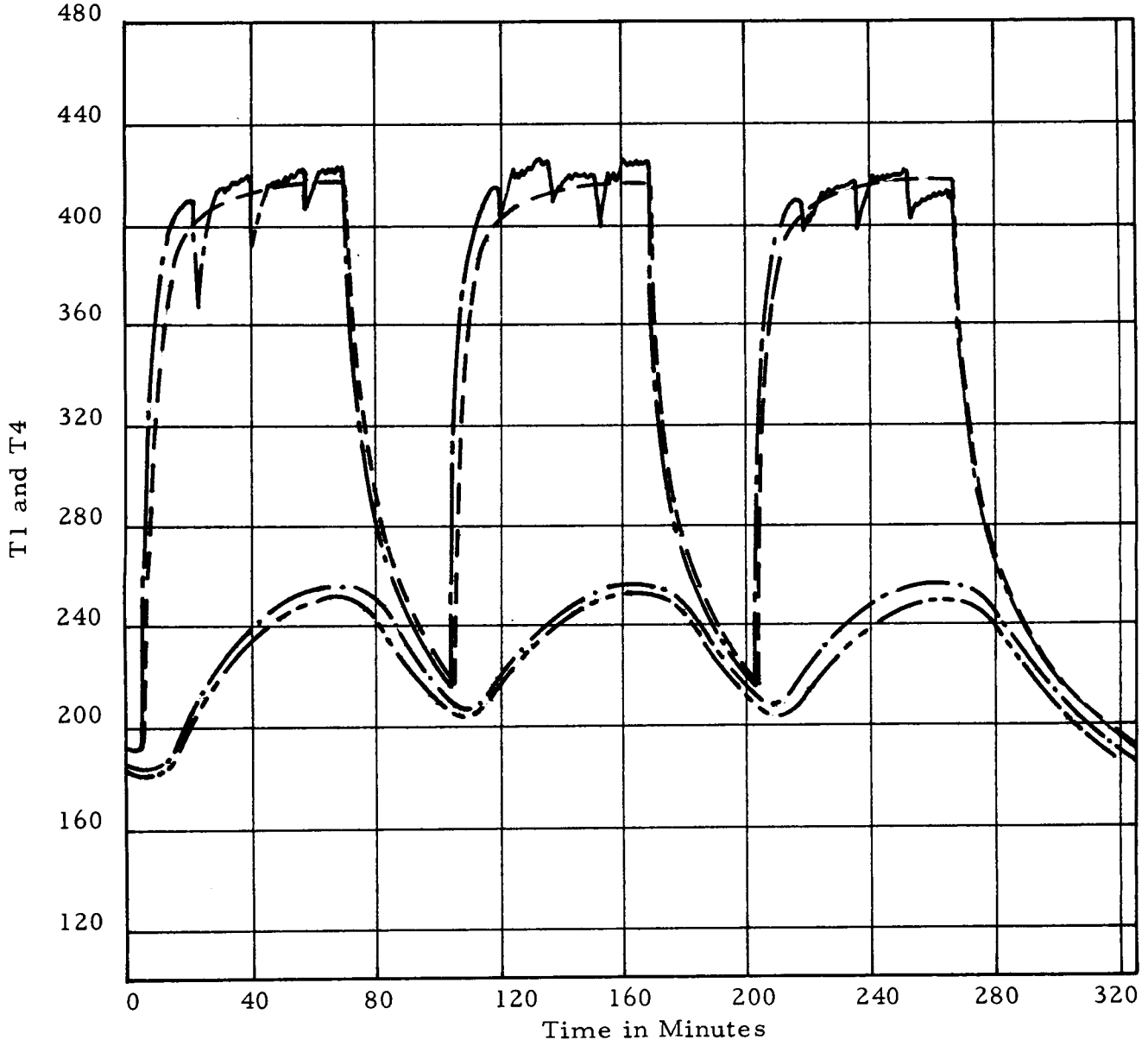

FIGURE 14 - MEASURED AND CALCULATED DETECTOR PANEL TEMPERATURES

Approximately 200 thermocouples were utilized in monitoring the canister, sink, and structure temperatures. They were placed on each electrical component, across various heat paths, etc. The sink and exterior structure temperatures, programmed at orbital extremes, were obtained by the use of heater blankets with an adjustable heating current system.

In the first series of runs, the battery temperatures were running at 266°K. These cold temperatures were found to result from excessive extraneous heat leaks. Several methods were employed to eliminate excessive heat leakage, one of which was wrapping the electronic harness with aluminized Mylar. In a later run, a minimum battery temperature of 281°K was obtained in the cold case. The time constant was verified at 15 hours.

All other specifications were met during these tests. A summary of the Pegasus-A thermal vacuum data follows.

CANISTER PROTOTYPE THERMAL VACUUM TEST

Test #1	Heat Dissipation	Ave. Internal Temp.	Battery Temp.
Hot Case	74	294°K	296°K
Cold Case	44	264	266
Test #2			
Hot Case	64.1	300	300
Cold Case	44.9	279	281

3. Laboratory Studies on Pegasus Thermal Control Coatings. Much effort was exerted in the evaluation in the laboratory of the space stability and optical properties of the Pegasus thermal control coatings. Studies were performed at Marshall Space Flight Center (both RPL and P&VE), Fairchild-Hiller Corporation, Schjeldahl, and Lockheed. Emphasis was placed on the Alodine and S-13 coatings because of their extreme importance to the success of the thermal design. Each was tested systematically to relate space degradation, manner of application, and prelaunch environmental effects (Table III).

The coatings were found to be extremely stable except that the S-13 did degradate after contamination. For this reason, the vehicle was washed just prior to countdown. Radiometric measurements were performed on the pad (Table IV).

C. QUICK-LOOK ORBITAL DATA FROM PEGASUS-A

Initially, the thermal behavior of the meteoroid detector panels was mild because of the rapid spin about the x-axis (Figure 15). As the spin gradually shifted to the y-axis, more extensive temperature variations occurred as the satellite passed in and out of the earth's shadow (Figure 16).

The SMA temperatures are approximately 40°K above predicted levels (Figure 17). Evaluation of these data is being performed to explain this phenomenon. Apparently, compensation by the louvers maintains the electronic temperatures at the desired level (Figure 18).

The variations in per cent time in sunlight per orbit have been calculated for the first year in the life of Pegasus-A and are shown in Figure 19. It can be seen that the first possible hot orbit occurred

TABLE III

LABORATORY RADIOMETRIC STUDIES ON ALODYNE (MTL-3)

THERMAL-VACUUM†				THERMAL-VACUUM†-ULTRAVIOLET‡							
Sample No.	ϵ_T Before	Temp °C	ϵ_T After	Sample No.	ϵ_T Before	α_s Before	Time ‡ESH	Temp °C	ϵ_T After	α_s After	$\Delta\alpha_s/\epsilon_T$
H	0.57	110	0.51	K	0.68	0.463	300	85	0.64	0.471	+0.055
	0.51	195	0.44								
				L	0.64	0.484	300	85	0.62	0.491	+0.042
I	0.57	110	0.47								
				M	0.58	0.505	300	60	0.58	0.514	+0.015
J	0.65	125	0.54								
				N	0.62	0.509	860	97	0.63	0.511	-0.010
				O	0.54	0.507	860	27	0.54	0.518	+0.020
				P	0.60	0.520	860	28	0.60	0.536	+0.026
				Q	0.67	0.451	1000	120	0.63	0.470	+0.073
				R	0.55	0.533	1000	137	0.52	0.543	+0.075
				S	0.51	0.531	1000	75	0.50	0.544	+0.047

† 10^{-5} Torr

‡ ESH = equivalent sun hours of ultraviolet (0.2 - 0.4 microns)

TABLE IV

SUMMARY OF SEVERAL ON-THE-PAD RADIOMETRIC SURVEYS ON PEGASUS-A

I. THE S-13 THERMAL CONTROL COATING (On the Service Module Adapter, Instrument Unit, and S-IV

A. Measurements of S-13 Coated Tabs placed near the Vehicle on-the-pad

1. $.22 \leq \alpha_s \leq .25$

2. $.82 \leq \epsilon_N \leq .88$

B. Measurements Made on the Service Module Adapter, Instrument Unit, and S-IV

1. $.16 \leq \alpha_s \leq .24$

2. $.81 \leq \epsilon_N \leq .86$

3. $.16 \leq \alpha_s \leq .19$ (measurements made just after vehicle was washed 7 days prior to launch)

II. THE ALODINE THERMAL CONTROL (On the Detector Panels)

A. Measurements Made on Alodine (MTL-3) Coated Tabs placed near Pegasus on-the-pad

1. $.51 \leq \alpha_s \leq .53$

2. $.53 \leq \epsilon_N \leq .58$

3. $\alpha_s/\epsilon_N \leq 1.0$

B. Measurements Made on the Detector Panels

1. $.50 \leq \alpha_s \leq .56$

2. $.53 \leq \epsilon_N \leq .65$

3. $\alpha/\epsilon \leq 1.0$

α_s Measurements were made with a Portable Gier Dunkle Reflectometer

ϵ_N Measurements were made with a Portable Lion Emittometer

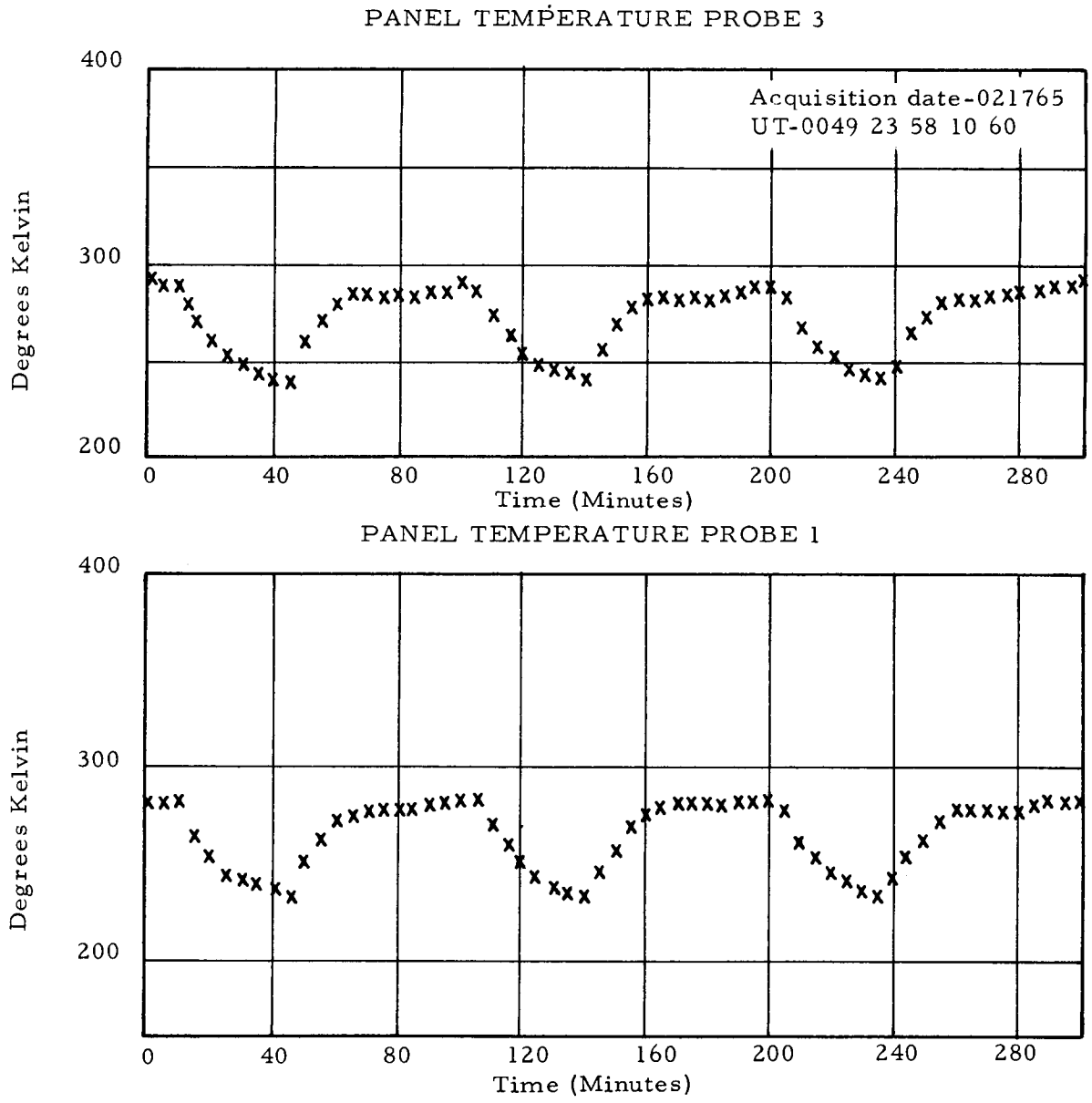

FIGURE 15 - EARLY DETECTOR PANEL ORBITAL DATA

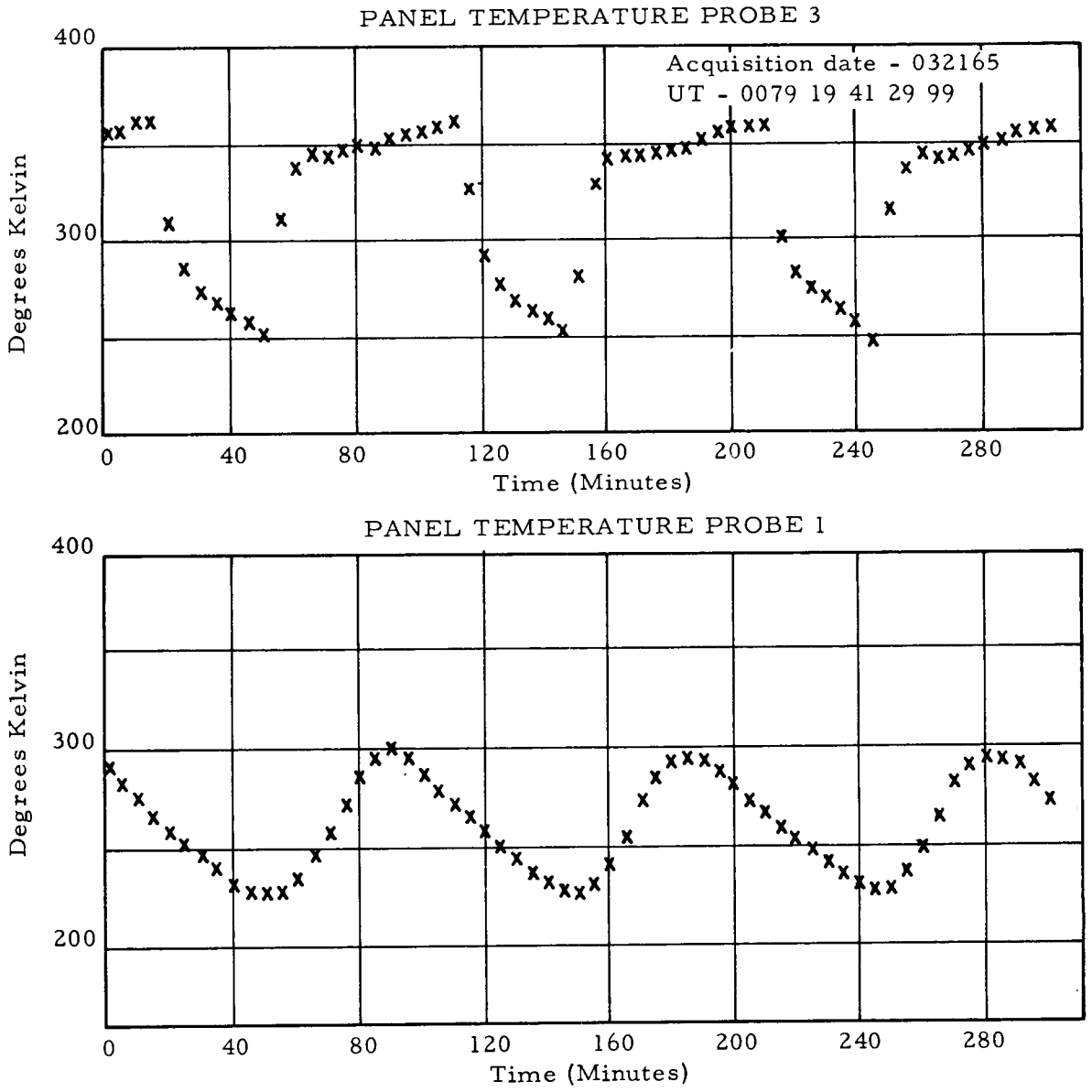

FIGURE 16 - LATER DETECTOR PANEL ORBITAL DATA

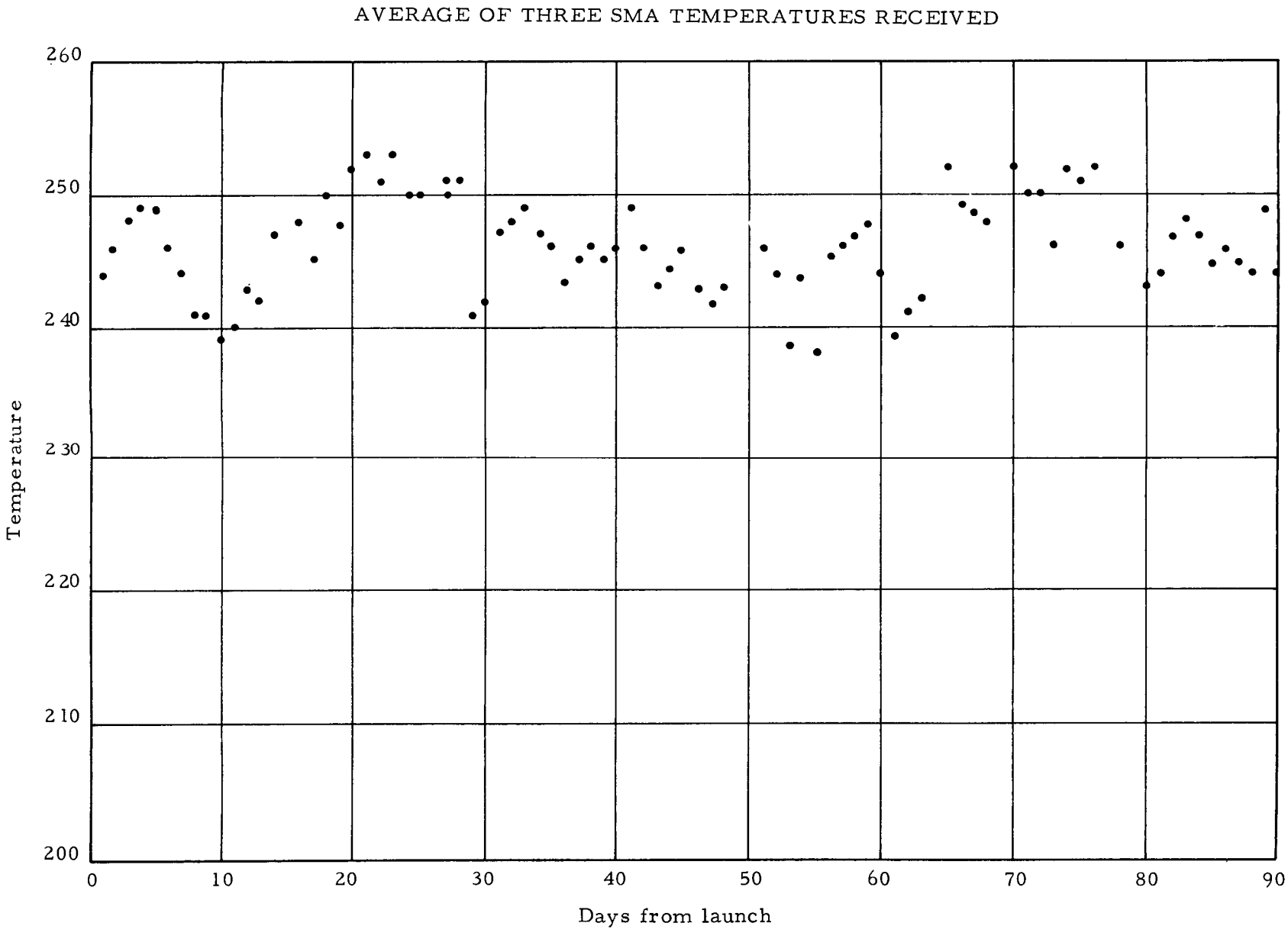

FIGURE 17 - AVERAGE SMA ORBITAL TEMPERATURES

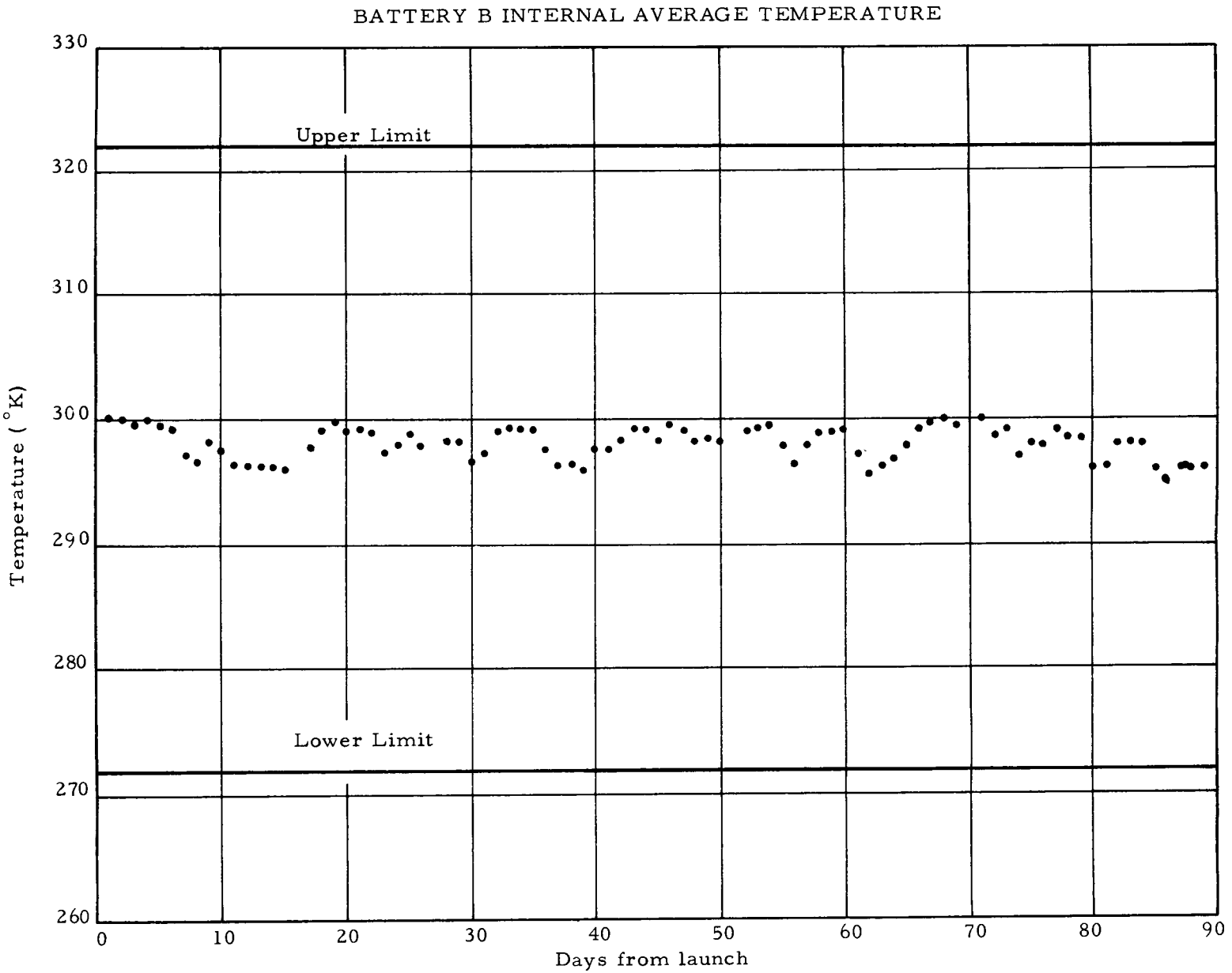

FIGURE 18 - BATTERY ORBITAL TEMPERATURE

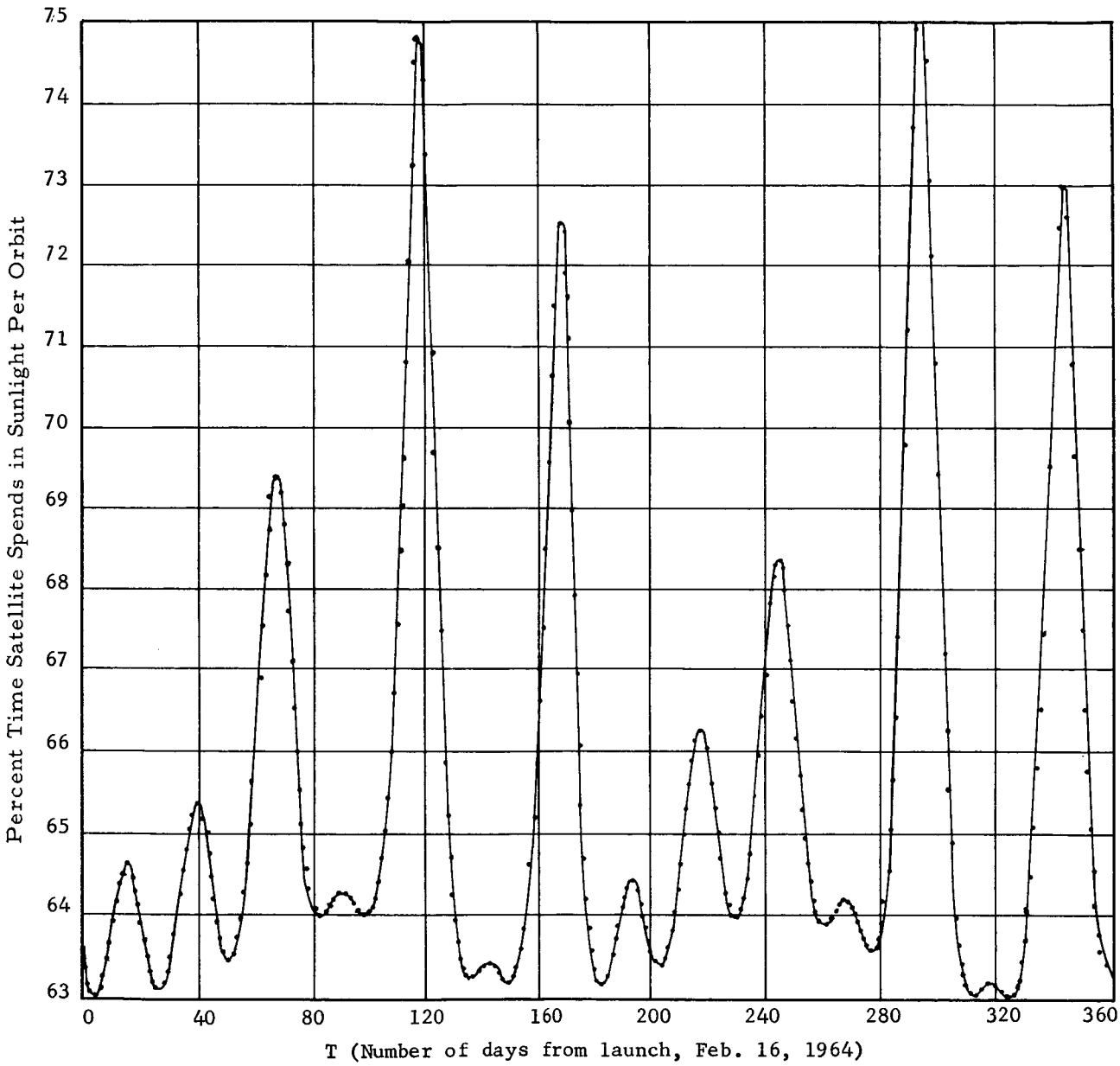

FIGURE 19 - TIME IN SUNLIGHT

about June 12 (116th day in orbit), when the per cent time in sunlight reached 74.8%, compared to the initial 64-65%.

A detailed evaluation of the thermal design is being performed.

APPENDIX I

Article I

The General Space Thermal Program[1]

This program includes subroutines for obtaining geometric and orbital parameters necessary to compute the many flux terms, and, simultaneously, solves a set of "n" calorimetric equations of the general form:

$$\dot{T}_i H_i = A_{1i}\,\alpha_i S + A_{2i}\,\alpha_i\,SB + A_{3i}\,\epsilon_i\,SE - A_{4i}\,\epsilon_i\,\sigma\left(\frac{T_i}{100}\right)^4 + \sum_{j=1}^{n}\left[C_{ij}\,T_j + R_{ij}\left(\frac{T_j}{100}\right)^4\right] - T_i\sum_{j=1}^{n} C_{ij} - \frac{T_i}{100}\sum_{j=1}^{n} R_{ij} + \dot{Q}_i$$

where

T_i = temp of node i

$\dot{T}_i = \frac{dTi}{dt}$

H_i = heat cap of node i

C_{ij} = conductance between nodes i and j

R_{ij} = radiance between nodes i and j

$\dot{Q}_i$ = internal heat of node i

[1] The general computer program was developed by Research Projects Lab (-T) and Computation Laboratory (-P).

α_1 = solar absorptance of node i

ϵ_1 = IR emittance of node i

S = insolation

B = max % of S for albedo

E = max % of S for earth's IR

σ = Stefan-Boltzmann constant

A_{1i} = area function for incident solar energy to node i

A_{2i} = area function for incident albedo energy to node i

A_{3i} = area function for incident earth IR to node i

A_{4i} = radiating area of node i

Article II

A Computer Program Describing the MMC Detector Panels

The functions incorporated into the "General Space Thermal Program" for study of the detector panels follow.

A. Area Functions

1. Solar

$A_{11} = A_{41}$ D cos (MAS)

$A_{11} = 0$ if MAS > 90°

$A_{12} = 0$

$A_{13} = 0$

$A_{14} = A_{44}$ D cos (180-MAS)

$A_{14} = 0$ if supp MAS > 90°

2. Albedo

$A_{21} = A_{41} (F_{\gamma_{1r}}) \cos (RAS)$

$A_{21} = 0$ if $RAS > 90^{\circ}$

$\gamma_1 = 180^{\circ} - RAM$

$A_{22} = 0$

$A_{23} = 0$

$A_{24} = A_{44} (F_{\gamma_{4r}}) \cos (RAS)$

$A_{24} = 0$ if $RAS > 90^{\circ}$

$\gamma_4 = RAM$

3. Earth's IR

$A_{31} = A_{41} F_{\gamma_{1r}}$

$A_{32} = 0$

$A_{33} = 0$

$A_{34} = A_{44} F_{\gamma_{4r}}$

4. Stefan-Boltzmann radiation

$A_{41} = 1$

$A_{42} = 0$

$A_{43} = 0$

$A_{44} = 1$

5. Generated Heat Fluxes

all $\dot{Q}i = 0$

6. Conductances

$C_{12} = C_{21} = 4.6$ kcal/hr°k

$C_{23} = C_{32} = 2.3$

$C_{34} = C_{43} = 1.4$

7. Heat Capacities

$H_1 = H_4 = .36$

$H_2 = H_3 = .22$

8. Orbital parameters (predicted)

Rp = 6778 km

i = 31.8°

e = .0076

Tx = 63 to 78

Ω = 0

ω = 90

Ps = 90

Article III

A Computer Program Describing the MMC Electronic Canister Thermal Design

Discussion

Several components of the micrometeoroid measurement capsule have critical temperature limits. Hence, the present program was developed to aid in the evaluation of the thermal design of the electronics canister.

Utilization is made of "The General Space Thermal Program" (GSTP) which includes orbital subroutines and an integration routine for a set of "n" calorimetric equations (Article I).

A new subroutine was added to GSTP to allow the satellite to tumble about $\vec{M}_o$, a fixed vector on the satellite. Runs for all important thermal case were made.

II. DESIGNATION OF ISOTHERMS (NODES) AND EQUATIONS

A. Nodes and Orientation Vectors

1. Vectors ($\vec{M}_k$)

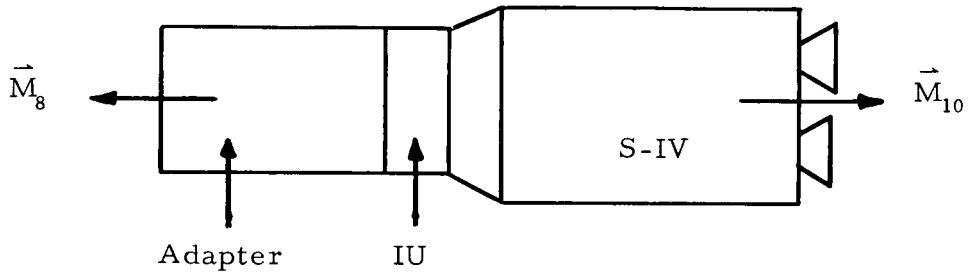

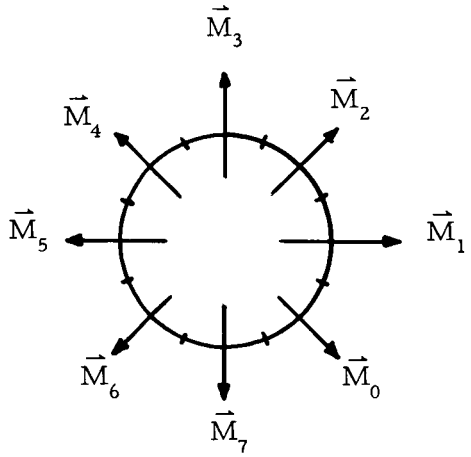

2. Nodes (i)

(a) adapter

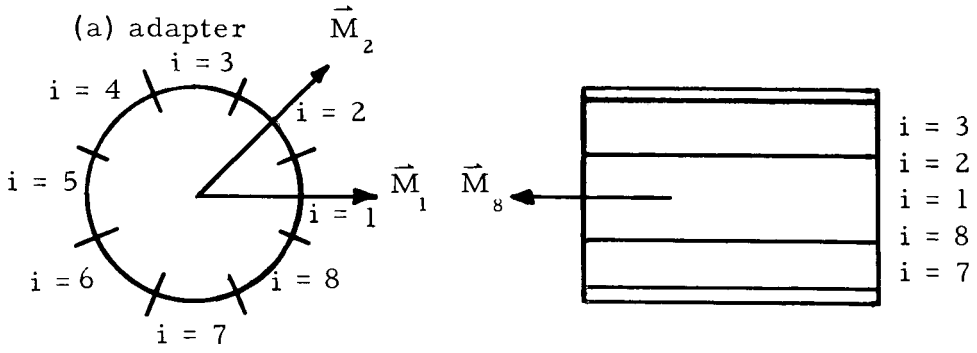

(b) IU

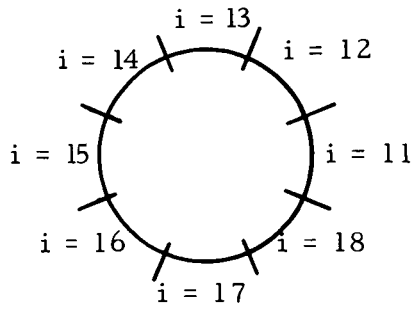

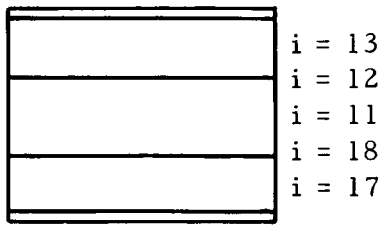

(c) Cylindrical Section of S-IV Stage

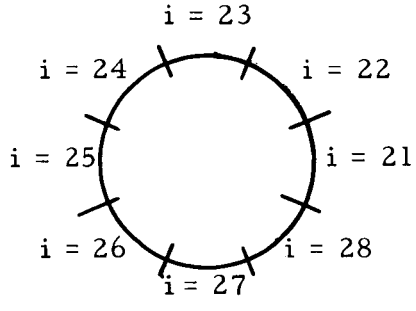

(d) Conical Section of S-IV Stage

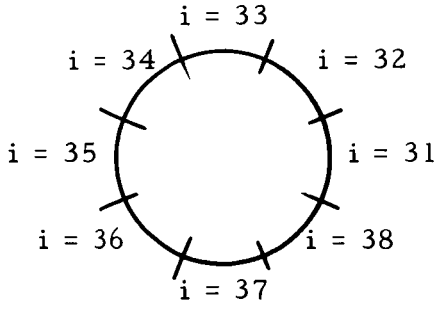

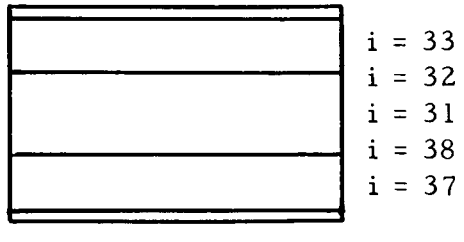

(e) Canister (outside layer)

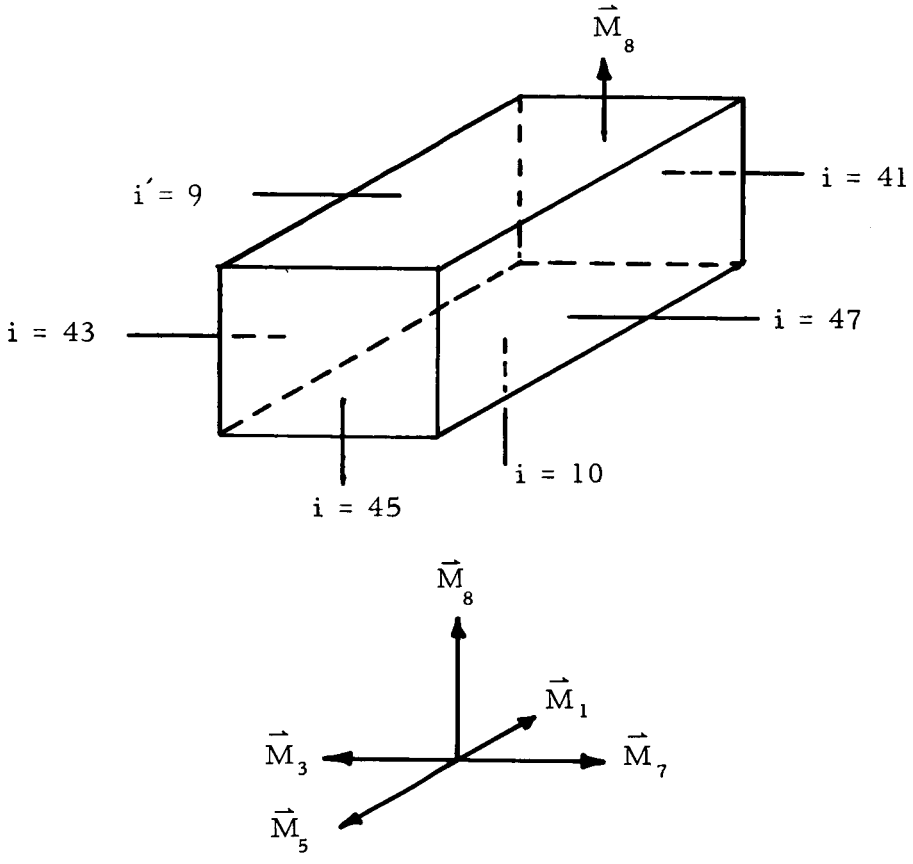

(f) Rear of S-IV Stage

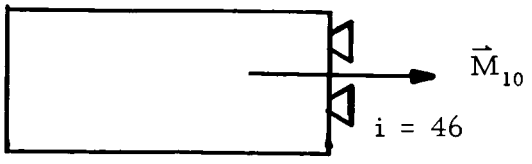

(g) Structure

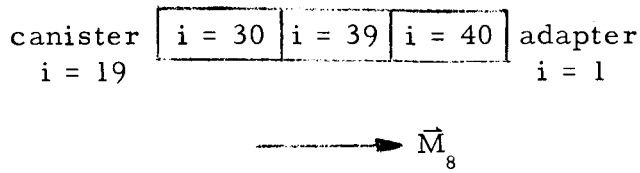

(h) Internal Nodes

($A_{4i} = 0$)

i = 10 bottom face of canister (not louvers)

i = 19 electronics components

i = 20 top S-IV bulkhead

i = 29 bottom of S-IV bulkhead

i = 42 louvers

B. Area Equations

The following parameters, used frequently in the area equations, are computer and stored each time step from initial input and/or previous time step.

D - shadow - sunlight step function

$(MAS)_k$ - angle between $\vec{M}_k$ and earth - sun vector

$(RAM)_k$ - angle between $\vec{M}_k$ and earth - satellite vector

(RAS) - angle between earth - sun vector and earth - satellite vector

$F_{\gamma r}$ - earth satellite radiation geometry factor

1. Those nodes whose area functions are similar in form and have $\vec{M}_1$ as their normal:

i = 11, 21, and 31

$A_{1i} = D\ A_{4i}\ \cos(MAS)_1$

$A_{1i} = 0$ if above is neg

$A_{2i} = F_{\gamma_1 r} \; A_{4i} \; \cos(\text{RAS})$

$A_{2i} = 0$ if above is neg

where $\gamma_1 = 180^\circ - (\text{RAM})_1$

$A_{3i} = F_{\gamma_1 r} \; A_{4i}$

A_{4i} = input constant

2. Those nodes whose area functions are similar in form and have $\vec{M}_2$ as their normal:

i = 12, 22, and 32

$A_{1i} = D A_{4i} \cos (\text{MAS})_2$

$A_{1i} = 0$ if above is neg.

$A_{2i} = F_{\gamma_{2r}} \; A_{4i} \cos (\text{RAS})$

$A_{2i} = 0$ if above is neg.

where $\gamma_2 = 180^\circ - (\text{RAM})_2$

$A_{3i} = F_{\gamma_{2r}} \; A_{4i}$

A_{4i} = input constant

3. Those nodes whose area functions are similar in form and have $\vec{M}_3$ as their normal:

i = 13, 23, and 33

$A_{1i} = D \; A_{4i} \cos (\text{MAS})_3$

$A_{1i} = 0$ if above is neg.

$A_{2i} = F_{\gamma_{3r}} \; A_{4i} \cos (\text{RAS})$

$A_{2i} = 0$ if above is neg.

where $\gamma_3 = 180^\circ - (\text{RAM})_3$

$A_{3i} = F_{\gamma_{3r}} A_{4i}$

A_{4i} = input constant

4. Those nodes whose area functions are similar in form and have $\vec{M}_4$ as their normal:

i = 14, 24, and 34

$A_{1i} = D A_{4i} \cos (MAS)_4$

$A_{1i} = 0$ if above is neg.

$A_{2i} = F_{\gamma_{4r}} A_{4i} \cos (RAS)$

$A_{2i} = 0$ if above is neg.

where $\gamma_4 = 180^\circ - (RAM)_4$

$A_{3i} = F_{\gamma_{4r}} A_{4i}$

A_{4i} = input constant

5. Those nodes whose area functions are similar in form and have $\vec{M}_5$ as their normal:

i = 15, 25, and 35

$A_{1i} = D A_{4i} \cos (MAS)_5$

$A_{1i} = 0$ if above is neg.

$A_{2i} = F_{\gamma_{5r}} A_{4i} \cos (RAS)$

$A_{2i} = 0$ if above is neg.

where $\gamma_5 = 180^\circ - (RAM)_5$

$A_{3i} = F_{\gamma_{5r}} A_{4i}$

A_{4i} = input constant

6. Those nodes whose area functions are similar in form and have $\vec{M}_6$ as their normal:

i = 16, 26, and 36

$A_{1i} = D\, A_{4i} \cos (MAS)_6$

$A_{1i} = 0$ if above is neg.

$A_{2i} = F_{\gamma_{6r}}\, A_{4i} \cos (RAS)$

$A_{2i} = 0$ if above is neg.

where $\gamma_6 = 180^\circ - (RAM)_6$

$A_{3i} = F_{\gamma_{6r}}\, A_{4i}$

A_{4i} = input constant

7. Those nodes whose area functions are similar in form and have $\vec{M}_7$ as their normal:

i = 17, 27, and 37

$A_{1i} = D\, A_{4i} \cos (MAS)_7$

$A_{1i} = 0$ if above is neg.

$A_{2i} = F_{\gamma_{7r}}\, A_{4i} \cos (RAS)$

$A_{2i} = 0$ if above is neg.

where $\gamma_7 = 180^\circ - (RAM)_7$

$A_{3i} = F_{\gamma_{7r}}\, A_{4i}$

A_{4i} = input constant

8. Those nodes whose area functions are similar in form and have $\vec{M}_0$ as their normal:

i = 18, 28, and 38

$A_{1i} = D_{\cdot} A_{4i} \cos (MAS)_0$

$A_{1i} = 0$ if above is neg.

$A_{2i} = F_{\gamma_{0r}} A_{4i} \cos (RAS)$

$A_{2i} = 0$ if above is neg.

where $\gamma_0 = 180^\circ - (RAM)_0$

$A_{3i} = F_{\gamma_{0r}} A_{4i}$

A_{4i} = input constant

9. Node #9 which has $\vec{M}_8$ as its normal:

$A_{1i} = D\, A_{4i} \cos (MAS)_8$

$A_{1i} = 0$ if above is neg.

$A_{2i} = F_{\gamma_{8r}} A_{4i} \cos (RAS)$

$A_{2i} = 0$ if above is neg.

where $\gamma_8 = 180^\circ - (RAM)_8$

$A_{3i} = F_{\gamma_{8r}} A_{4i}$

A_{4i} = input constant

10. Node #20 which has $\vec{M}_8$ as its normal:

Note: An imperical method was used to account for shadow effects of the adapter

$A_{1i} = (10)\, D\, A_{4i} \cos (MAS)_8 \cos\left[3(MAS)_8\right]$ if $(MAS)_8 \leq 30^\circ$

$A_{1i} = 0$ if $(MAS)_8 > 30^\circ$

$A_{2i} = (7)\, F_{\gamma_{8r}} A_{4i} \cos (RAS)$

$A_{2i} = 0$ if $\cos(RAS) > 0^\circ$

$A_{2i} = 0$ if $\gamma_8 \geq 30^\circ$

$A_{3i} = (7)\ F_{\gamma_8 r}\ A_{4i}$

$A_{3i} = 0$ if $\gamma_8 \geq 30^\circ$

A_{4i} = input constant

11. Node #46 which has $\vec{M}_{10}$ as its normal:

$\alpha m_{10} = 180^\circ - \alpha m_8$

$\delta m_{10} = -\delta m_8$

$A_{1i} = D\ A_{4i} \cos (MAS)_{10}$

$A_{1i} = 0$ if above is neg.

$A_{2i} = F_{\gamma_{10} r}\ A_{4i} \cos (RAS)$

$A_{2i} = 0$ if above is neg.

where $\gamma_{10} = 180^\circ - (RAM)_{10}$

$A_{3i} = F_{\gamma_{10} r}\ A_{4i}$

A_{4i} = input constant

12. The adapter nodes, i = 1, 2, ---, 8, which have $\vec{M}_1$, $\vec{M}_2$, $\vec{M}_3$, $\vec{M}_4$, $\vec{M}_5$, $\vec{M}_6$, $\vec{M}_7$, and $\vec{M}_0$ as their respective normals:

Note: b_i and e_i are empirical. For i = 8, the $\underline{i} = 0$.

$A_{1i} = a_i + b_i$

$A_{2i} = c_i$

$A_{3i} = d_i + e_i$

$A_{4i} = f_i + g_i/_4$

where

$a_i = D\ f_i \cos (MAS)_{\underline{i}}$

$a_i = 0$ if above is neg.

$b_i = 2\ D\ f_i\ h_i \cos (MAS)_8 \cos (180^\circ - MAS_i)$

$b_i = 0$ if either $\cos (MAS)_8 < 0$ or $\cos (180^\circ - MAS_i) < 0$

$c_i = (d_i + d_i) \cos (RAS)$

$c_i = 0$ if above is neg.

$d_i = F_{\gamma_{ir}}\ f_i$

$e_i = F\ (RAM_i)r\ g_i (\cos[180 - RAM_8])^{\frac{1}{2}}$

$e_i = 0$ if above is neg.

f_i = input constant (the actual area of one side)

g_i = input constant $\left(\frac{\epsilon \text{inside}}{\epsilon \text{outside}}\right)$ times f_i

h_i = input constant $\left(\frac{\alpha \text{inside}}{\alpha \text{outside}}\right)$

13. The canister wall nodes, i = 41, 43, 45, and 47, whose normals are $\vec{M}_1$, $\vec{M}_3$, $\vec{M}_5$, and $\vec{M}_7$, respectively.

$A_{1i} = D\ A_{4i} \cos (MAS)_k$

$A_{1i} = 0$ if above is neg.

$A_{1i} = 0$ if $(MAS)_8 > 90^\circ$

$A_{2i} = F_{\gamma_k r}\ A_{4i} \cos (RAS)$

$A_{2i} = 0$ if above is neg.

$A_{2i} = 0$ if $(MAS)_8 > 90^\circ$

where $\gamma_k = 180^\circ - (RAM)_k$

$A_{3i} = F_{\gamma_k r}\ A_{4i}$

$A_{3i} = 0$ if $(RAM)_8 > 90^\circ$

A_{4i} = input constant (.5 actual area)

Note: Remember k is the subscript in $\vec{M}_k$

14. The structure nodes, i = 30, 39, and 40 whose axis is $\vec{M}_8$:

$$A_{1i} = (.9)\frac{A_{4i}}{\pi} \sin (MAS)_8$$

$$A_{2i} = (.9)\, F_{\gamma_{8r}} \left|A_{4i/\pi}\right| \cos (RAS)$$

$A_{2i} = 0$ if above is neg.

$$A_{3i} = (.9)\, F_{\gamma_{8r}}\, A_{4i/\pi}$$

A_{4i} = input constant

III. ORBITAL AND THERMAL COEFFICIENTS

The temperature of the electronics canister, T_{19}, is a function of all the orbital and thermal coefficients. For many coefficients, it is a very weak function. The purpose of this program is: (1) to combine all the inputs for T_{19}, and (2) to evaluate the effect of certain coefficients on T_{19} parametrically, especially those coefficients which have large probable errors.

The coefficients for the first run follow.

A. Areas (m^2)

1. Adapter nodes, i = 1, 2, ---, 8

$$f_i = \frac{\pi dl}{8} = \frac{(3.14)\,(3.91)\,(2.34)}{8} = 3.59\ m^2$$

$$g_i = (3.59)\,(1) = 3.59$$

$$h_i = .5/.3 = 1.67$$

2. IU nodes, i = 11, 12, ---, 18

$$A_{4i} = \frac{\pi dl}{8} = \frac{(3.14)(3.91)(1.47)}{8} = 2.26$$

3. S-IV conical nodes,

i = 31, 32, ---, 38

$$A_{4i} \cong \frac{\pi \bar{d} l}{8} = \frac{(3.14)(4.75)(3.94)}{8} = 7.35$$

4. S-IV cylindrical nodes, i = 21, 22, ---, 28

$$A_{4i} = \frac{\pi dl}{8} = 26.8$$

5. S-IV tail section node, i = 46

$$A_{4i} = \pi r^2 = (3.14)(2.79)^2 = 24.5$$

6. S-IV bulkhead node, i = 20

$$A_{4i} = \frac{\pi r^2}{10} = 1.2$$

7. Top of canister node, i = 9

$$A_{4i} = l\,w = .52$$

8. End of canister nodes, i = 41 and 45

$$A_{4i} = l\,w = .34$$

9. Side of canister nodes, i = 43 and 47

$$A_{4i} = l\,w = .67$$

10. Structural nodes, i = 30, 39, and 40

$$A_{4i} \cong \frac{1}{2} (\pi)(d)(l)(\#\ \text{tubes}) = .94$$

B. Heat Capacities (Joules/$^{\circ}$K)

1. Adapter nodes, i = 1, 2, ---, 8

$M \cong \frac{2100 \text{ lb}}{8} = 120 \text{ kgm}$

$H = (120)\ (937 \text{ Joules/kgm}^{\circ}\text{K})$

$H = 1.12 \times 10^{5}$

2. IU nodes, i = 11, 12, ---, 18

$M \cong \frac{2500 \text{ lb}}{8} = 142 \text{ kgm}$

$H = 1.33 \times 10^{5}$

Note: Many weights will change slightly.

3. S-IV conical nodes, i = 31, 32, ---, 38

$M \cong 115 \text{ kgm}$

$H = 1.08 \times 10^{5}$

4. S-IV cylindrical nodes, i = 21, 22, ---, 28

$M \cong 306 \text{ kgm}$

$H = 2.87 \times 10^{5}$

5. S-IV bulkhead node, i = 20

$M \cong 919 \text{ kgm}$

$H = 8.61 \times 10^{5}$

6. S-IV tail section node, i = 46

$M \cong 1840 \text{ kgm}$

$H = 1.72 \times 10^{6}$

7. Structural nodes, i = 30, 39, and 40

$H = 7.6 \times 10^3$

8. Canister nodes, i = 41, 43, 45, 47, 9, 10, and 19

$H_{41}\left[= H_{43} = H_{45} = H_{47} = H_9 = H_{10}\right]$

$H_{41} = 20$

Note: The preceding nodes represent a thin foil whose heat capacity is actually much lower than 20 Joules/°K. However, H = 20 is the smallest value consistent with reasonable time steps with which the Runge-Kutta numerical integration converges.

$M_{19} \cong 61.3$ kg

$H_{19} = 57.4 \times 10^3$

$M_{42} = \frac{1.8 \text{ lb}}{2.2} = .82$ kg

$H_{42} = 7.7 \times 10^2$

C. Conductances (watts/°K)

1. Between adapter nodes

$C_{12}, C_{23}, C_{34}, C_{45}, C_{56}, C_{67}, C_{78}, C_{18}$

$C = \frac{kA}{l}$

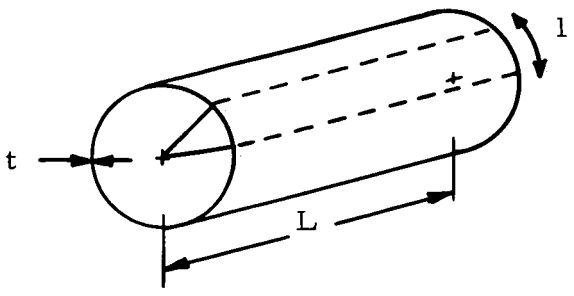

$A = L\,t$

$C = 1.27$

2. Between adapter and IU nodes

$C_{1\,(11)}$; $C_{2(12)}$, $C_{3(13)}$, $C_{4(14)}$, $C_{5(15)}$, $C_{6(16)}$, $C_{7(17)}$, and $C_{8(18)}$

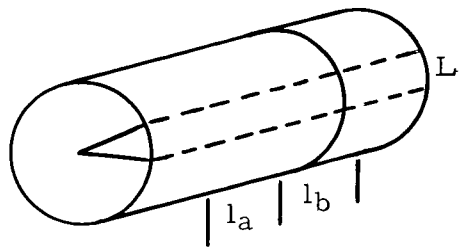

$$\frac{1}{C} = \frac{1}{C_a} + \frac{1}{C_b}$$

$C_a = k A_a / l_a = 1.10$

$C_b = k A_b / l_b = .554$

$C = .369$

3. Between IU nodes

$C_{11(12)}$, $C_{12(13)}$, $C_{13(14)}$, $C_{14(15)}$, $C_{15(16)}$, $C_{16(17)}$, $C_{17(18)}$, $C_{11(18)}$

$C = k A / L$

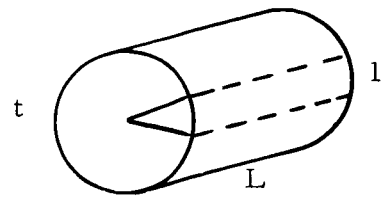

$A = L\,t$

$C = .160$

4. Between IU and S-IV conical nodes

$C_{11(31)}$, $C_{12(32)}$, $C_{13(33)}$, $C_{14(34)}$, $C_{15(35)}$, $C_{16(36)}$, $C_{17(37)}$, $C_{18(38)}$

$$\frac{1}{C} = \frac{1}{C_a} + \frac{1}{C_b}$$

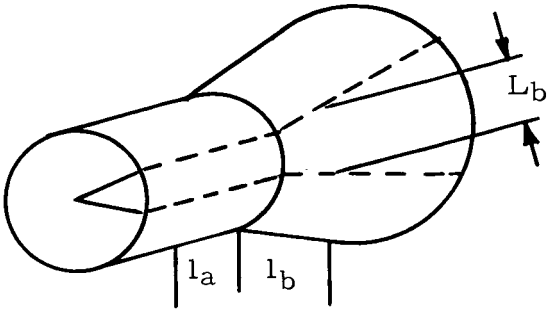

$C_a = k A_a / l_a$

$C_b = k A_b / l_b$

$C = .146$

5. Between S-IV conical nodes

$C_{31(32)}$, $C_{32(33)}$, $C_{33(34)}$, $C_{34(35)}$, $C_{35(36)}$, $C_{36(37)}$, $C_{37(38)}$ $C_{18(38)}$

$C = k A / l$

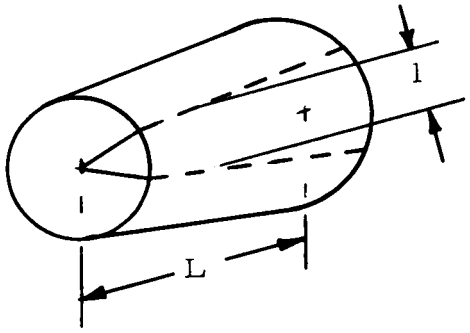

$C = .443$

6. Between S-IV conical and S-IV cylindrical nodes

$C_{21(31)}$, $C_{22(32)}$, $C_{23(33)}$, $C_{24(34)}$, $C_{25(35)}$, $C_{26(36)}$, $C_{27(37)}$ $C_{28(38)}$

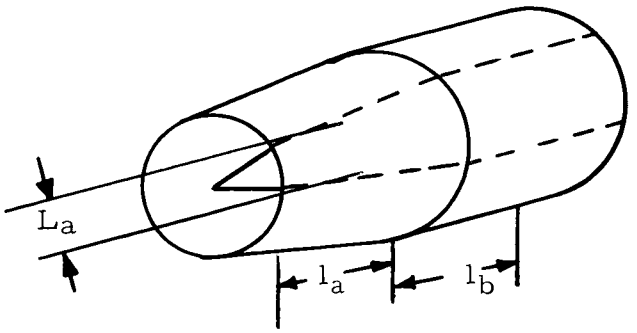

$$\frac{1}{C} = \frac{1}{C_a} + \frac{1}{C_b}$$

$C_a = kA_a/l_a$

$C = kA_b/l_b$

$C = .099$

7. Between S-IV cylindrical nodes

$C_{21(22)}$, $C_{22(23)}$, $C_{23(24)}$, $C_{24(25)}$, $C_{25(26)}$, $C_{26(27)}$, $C_{27(28)}$, and $C_{21(28)}$

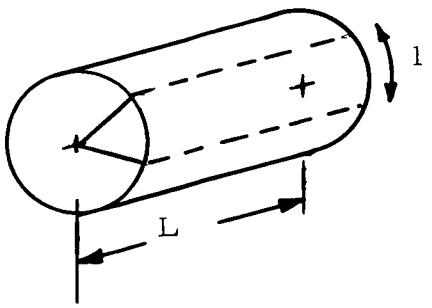

$C = kA/l$

$C = 3.05$

8. Between S-IV cylindrical and S-IV tail section nodes

$C_{21(46)}$, $C_{22(46)}$, $C_{23(46)}$, $C_{24(46)}$, $C_{25(46)}$, $C_{26(46)}$, $C_{27(46)}$, $C_{28(46)}$

Note: estimation

$C = \sim .1$

9. Between canister nodes

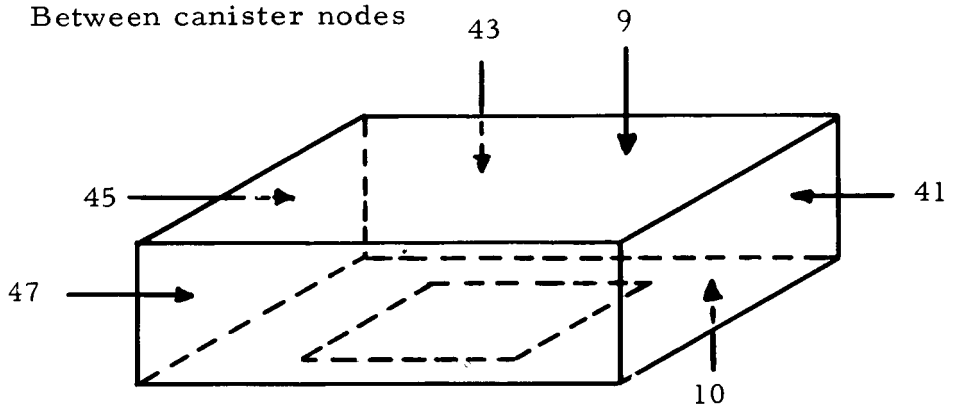

19 on inside assumed isothermal for this program

(a) $C_{9(19)}$

$C = kA/l$

$C = .08$

(b) $C_{10(19)}$

$C = kA/l$

$C = 0$ Note: area of louvers was increased until $A_{10} = 0$

(c) $C_{19(41)}$, $C_{19(45)}$

$C = kA/l$

$C = .04$

(d) $C_{19(43)}$, $C_{19(47)}$

$C = .12$

10. Between S-IV bulkhead nodes

$C_{20(29)} = 0$

11. Between structural nodes

(a) $C_{30(39)}$, $C_{39(40)}$

$C = kA/l = 2.4$

(b) $C_{1(40)}$

$C = 5$

(c) $C_{19(30)}$

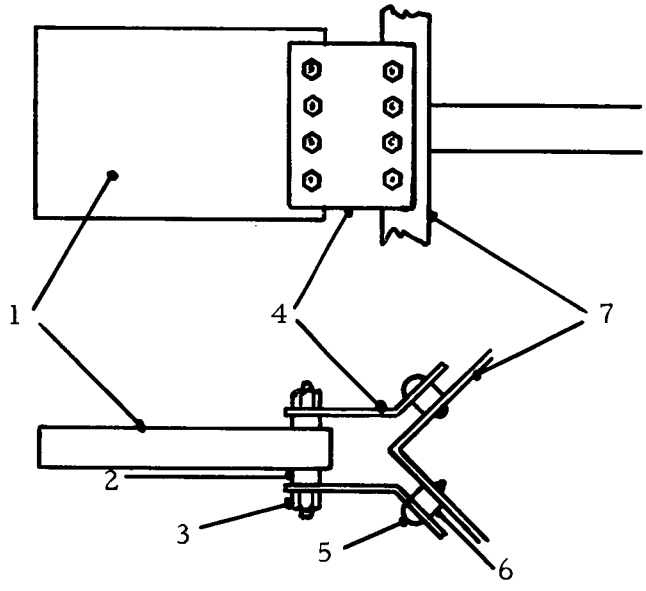

(1) panel

(2) thermal washer

(3) nut and bolt

(4) clip (fiberglass)

(5) rivet

(6) thermal washer

(7) support

$$\frac{1}{C} = \frac{1}{C_1 + C_2} + \frac{1}{C_3} + \frac{1}{C_4 + C_5} + \frac{1}{C_6}$$

C_1 = conductance thru thermal washer

C_2 = conductance thru bolt

C_3 = conductance thru clip

C_4 = conductance thru rivet

C_5 = conductance thru thermal washer

C_6 = conductance thru structure (node 30)

Note: there are eight clips

$C = .2$

D. Radiances (watts/$^\circ K^4$)

1. Involving canister (all equal R_{ij}'s are grouped). Also, the louvers control the canister temperature by controlling $R_{i(19)}$'s. Extreme values are presented as the hot and cold cases in (i) and (j).

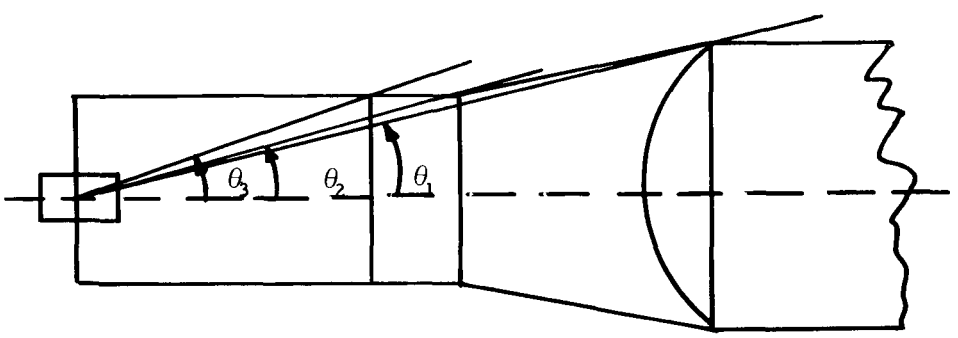

$\theta_1 = .35$ rad

$\theta_2 = .47$ rad

$\theta_3 = .70$ rad

G = % energy in the solid angle

$$G_{ij} = \int_{\theta_i}^{\theta_\gamma} 2 \sin\theta \cos\theta \, d\theta = \left[\sin^2\theta\right]_{\theta_i}^{\theta_\gamma}$$

$\theta_0 = 0$ to θ_1 $\quad G_{01} = .12$

θ_1 to θ_2 $\quad G_{12} = .09$

$G_{23} = .21$

$G_{34} = .59$

(a) $R_{1(10)}$, $R_{2(10)}$, $R_{3(10)}$, $R_{4(10)}$, $R_{5(10)}$, $R_{6(10)}$, $R_{7(10)}$, $R_{8(10)}$

$$R = \frac{G_{34} A\epsilon\sigma}{8} = .017$$

(b) $R_{10(11)}$, $R_{10(12)}$, $R_{10(13)}$, $R_{10(14)}$, $R_{10(15)}$, $R_{10(16)}$, $R_{10(17)}$, $R_{10(18)}$

$$R = \frac{G_{23} A\epsilon\sigma}{8} = .0060$$

(c) $R_{10(31)}$, $R_{10(32)}$, $R_{10(33)}$, $R_{10(34)}$, $R_{10(35)}$, $R_{10(36)}$, $R_{10(37)}$, $R_{10(38)}$

$$R = \frac{G_{12} A\epsilon\sigma}{8} = .0025$$

(d) $R_{10(20)}$

$$R = G_{01} A\epsilon\sigma = .027$$

(e) $R_{1(41)}$, $R_{5(45)}$

$$R \sim .2 A\epsilon\sigma = .038$$

(f) $R_{2(41)}$, $R_{4(45)}$, $R_{6(45)}$, $R_{8(41)}$

$$R \sim .15 A\epsilon\sigma = .028$$

(g) $R_{3(43)}$, $R_{7(47)}$

$R \sim .2\, A\epsilon\sigma = .076$

(h) $R_{2(43)},\ R_{4(43)},\ R_{6(47)},\ R_{8(47)}$

$R \sim .15\, A\epsilon\sigma = .057$

(i) Hot Case (louvers fully open)

1 $R_{1(19)},\ R_{2(19)},\ R_{3(19)},\ R_{4(19)},$

$R_{5(19)},\ R_{6(19)},\ R_{7(19)},\ R_{8(19)}$

$$R = \frac{G_{34}\, A\epsilon\sigma}{8} = .084$$

2 $R_{11(19)},\ R_{12(19)},\ R_{13(19)},\ R_{14(19)}$

$R_{15(19)},\ R_{16(19)},\ R_{17(19)},\ R_{18(19)}$

$$R = \frac{G_{23}\, A\epsilon\sigma}{8} = .030$$

3 $R_{31(19)},\ R_{32(19)},\ R_{33(19)},\ R_{34(19)}$

$R_{35(19)},\ R_{36(19)},\ R_{37(19)},\ R_{38(19)}$

$$R = \frac{G_{12}\, A\epsilon\sigma}{8} = .013$$

4 $R_{19(20)}$

$R = G_{01}\, A\epsilon\sigma = .014$

5 $R_{i(42)} = 0$ all i

(j) Cold Case (louvers fully closed)

1 $R_{19(i)} = 0$ i = 1 thru 8, 11 thru 18,
31 thru 38, 20

$\underline{2}$ $R_{1(42)}$, $R_{2(42)}$, $R_{3(42)}$, $R_{4(42)}$

$R_{5(42)}$, $R_{6(42)}$, $R_{7(42)}$, $R_{8(42)}$

R = .019

$\underline{3}$ $R_{11(42)}$, $R_{12(42)}$, $R_{13(42)}$, $R_{14(42)}$

$R_{15(42)}$, $R_{16(42)}$, $R_{17(42)}$, $R_{18(42)}$

R = .0069

$\underline{4}$ $R_{31(42)}$, $R_{32(42)}$, $R_{33(42)}$, $R_{34(42)}$,

$R_{35(42)}$, $R_{36(42)}$, $R_{37(42)}$, $R_{38(42)}$

R = .0029

$\underline{5}$ $R_{20(42)}$

R = .004

$\underline{6}$ $R_{19(42)}$

R = .264

2. $R_{i\gamma}$ not involving canister directly; most of these are derived by approximations.

(a) R_{12}, R_{13}, R_{14}, R_{15}, R_{16}, R_{17}, R_{18}, R_{23},

R_{24}, R_{25}, R_{26}, R_{27}, R_{28}, R_{34}, R_{35}, R_{36},

R_{37}, R_{38}, R_{45}, R_{46}, R_{47}, R_{48}, R_{56}, R_{57},

R_{58}, R_{67}, R_{68}, R_{78}.

$R \sim .08$ $A\epsilon\sigma = 1.4$

(b) $R_{1(14)}$, $R_{1(16)}$, $R_{2(15)}$, $R_{2(17)}$, $R_{3(16)}$,

$R_{3(18)}$, $R_{4(17)}$, $R_{4(11)}$, $R_{5(12)}$, $R_{5(18)}$,

$\underline{R_{6(11)}, R_{6(13)}, R_{7(12)}, R_{7(14)}, R_{8(13)}, R_{8(15)}}$

$R \sim (.01)$ $A\epsilon\sigma = .2$

(c) $R_{1(15)}$, $R_{2(16)}$, $R_{3(17)}$, $R_{4(18)}$,

$\underline{R_{5(11)}, R_{6(12)}, R_{7(13)}, R_{8(14)}}$

$R \sim (.02)$ $A\epsilon\sigma = .4$

(d) $R_{1(20)}$, $R_{2(20)}$, $R_{3(20)}$, $R_{4(20)}$

$\underline{R_{5(20)}, R_{6(20)}, R_{7(20)}, R_{8(20)}}$

$R \sim (.14)$ $A\epsilon\sigma = 2.5$

(e) $R_{11(12)}$, $R_{11(13)}$, $R_{11(14)}$, $R_{11(15)}$, $R_{11(16)}$,

$R_{11(17)}$, $R_{11(18)}$, $R_{12(13)}$, $R_{12(14)}$, $R_{12(15)}$,

$R_{12(16)}$, $R_{12(17)}$, $R_{12(18)}$, $R_{13(14)}$, $R_{13(15)}$,

$R_{13(16)}$, $R_{13(17)}$, $R_{13(18)}$, $R_{14(15)}$, $R_{15(16)}$,

$\underline{R_{15(17)}, R_{15(18)}, R_{16(17)}, R_{16(18)}, R_{17(18)}}$

$R \sim (.7)$ $A\epsilon\sigma = .7$

(f) $R_{11(34)}$, $R_{11(36)}$, $R_{12(35)}$, $R_{12(37)}$,

$R_{13(36)}$, $R_{13(38)}$, $R_{14(37)}$, $R_{14(31)}$,

$R_{15(38)}$, $R_{15(32)}$, $R_{16(31)}$, $R_{16(33)}$,

$R_{17(32)}$, $R_{17(34)}$, $R_{18(33)}$, $R_{18(35)}$

$R \sim (.01)$ $A\epsilon\sigma = .12$

(g) $R_{11(35)}$, $R_{12(36)}$, $R_{13(37)}$, $R_{14(38)}$,

$R_{15(31)}$, $R_{16(32)}$, $R_{17(33)}$, $R_{18(34)}$

$R \sim (.03)$ $A\epsilon\sigma = .35$

(h) $R_{11(20)}$, $R_{12(20)}$, $R_{13(20)}$, $R_{14(20)}$,

$R_{15(20)}$, $R_{16(20)}$, $R_{17(20)}$, $R_{18(20)}$

$R \sim (.25)$ $A\epsilon\sigma = 2.9$

(i) $R_{20(30)}$, $R_{20(32)}$, $R_{20(33)}$, $R_{20(34)}$,

$R_{20(35)}$, $R_{20(36)}$, $R_{20(37)}$, $R_{20(38)}$

$R \sim (.7)$ $A\epsilon\sigma = 25$

(j) $R_{21(22)}$, $R_{21(23)}$, $R_{21(24)}$, $R_{21(25)}$, $R_{21(26)}$,

$R_{21(27)}$, $R_{21(28)}$, $R_{22(23)}$, $R_{22(24)}$, $R_{22(25)}$, $R_{22(26)}$,

$R_{22(27)}$, $R_{22(28)}$, $R_{23(24)}$, $R_{23(25)}$, $R_{23(26)}$, $R_{23(27)}$,

$R_{23(28)}$, $R_{24(25)}$, $R_{24(26)}$, $R_{24(27)}$, $R_{24(28)}$, $R_{25(26)}$,

$R_{25(27)}$, $R_{25(28)}$, $R_{26(27)}$, $R_{26(28)}$, $R_{27(28)}$

$R \sim (.1)\ A\epsilon\sigma = 10$

(k) $R_{21(29)}$, $R_{22(29)}$, $R_{23(29)}$, $R_{24(29)}$, $R_{25(29)}$,

$R_{26(29)}$, $R_{27(29)}$, $R_{28(29)}$, $R_{21(46)}$, $R_{22(46)}$,

$R_{23(46)}$, $R_{24(46)}$, $R_{25(46)}$, $R_{26(46)}$, $R_{27(46)}$, $R_{28(46)}$

$R \sim (.15)\ A\epsilon\sigma = 15$

(l) $R_{31(32)}$, $R_{31(33)}$, $R_{31(34)}$, $R_{31(35)}$, $R_{31(36)}$,

$R_{31(37)}$, $R_{31(38)}$, $R_{32(33)}$, $R_{32(34)}$, $R_{32(35)}$, $R_{32(36)}$,

$R_{32(37)}$, $R_{32(38)}$, $R_{33(34)}$, $R_{33(35)}$, $R_{33(36)}$, $R_{33(37)}$,

$R_{33(38)}$, $R_{34(35)}$, $R_{34(36)}$, $R_{34(37)}$, $R_{34(38)}$, $R_{35(36)}$,

$R_{35(37)}$, $R_{35(38)}$, $R_{36(37)}$, $R_{36(38)}$, $R_{37(38)}$

$R \sim (.02)\ A\epsilon\sigma = .7$

E. Absorptances and Emittances

1. Surfaces with S-13

i = 1, 2, 3, 4, 5, 6, 7, 8, 11, 12, ---, 18,
21, 22, ---, 28, 31, 32, ---, 38.

cold case	hot case
$\alpha_i = .18$	$\alpha_i = .27$
$\epsilon_i = .9$	$\epsilon_i = .9$

2. Aluminum Surfaces

i = 9, 10, 30, 39, 40, 41, 43, 45

$\alpha_i = .2$

$\epsilon_i = .1$

3. Zinc Chromate Surfaces

$i = 20$

$\alpha_i = .5$

$\epsilon_i = .8$

4. Mixed Surfaces

$i = 46$

$\alpha_i = .6$

$\epsilon_i = .5$

F. Other Input Data (orbital parameters, computer keys, etc.)

$n = 47$	T_{19} initial = 300
$e = .054$	other T initial = 250
$i = 32^\circ$	$45 \leq Q_{19} \leq 62$
$R_o = 6378$	PCOEFF = 9.968×10^{-3}
$R_p = 6878$	10 rev
$\sigma = 5.67$	$\Gamma_1 = 45$
$S = 1400$	$\Psi_1 = 270$
$B = .44$	$P_1 = 0$
$E = .174$	$\Gamma_2 = 0$
$T_x = 85$	$\Psi_2 = 270$
$\Omega = 0$	$P_2 = 0$
$\omega = 90$	$\Gamma_3 = -45$
$\alpha_{mo} = 90$	$\Psi_3 = 270$
$\delta_{mo} = 0$	$P_3 = 0$
$\alpha_s = 0$	$\Gamma_4 = -90$
$\delta_s = 0$	$\Psi_4 = 0$
	$P_4 = 0$

$\Gamma_5 = -45$

$\Psi_5 = 90$

$P_5 = 0$

$\Gamma_6 = 0$

$\Psi_6 = 90$

$P_6 = 0$

$\Gamma_7 = 45$

$\Psi_7 = 90$

$P_7 = 0$

$\Gamma_8 = 0$

$\Psi_8 = 0$

$P_8 = 0$

APPROVAL TMX-53300

PEGASUS THERMAL DESIGN

by

Tommy C. Bannister

The information in this report has been reviewed for security classification. Review of any information concerning Department of Defense or Atomic Energy Commission programs has been made by the MSFC Security Classification Officer. This report, in its entirety, has been determined to be unclassified.

This document has also been reviewed and approved for technical accuracy.

Gerhard B. Heller

GERHARD HELLER
Deputy Director, Research Projects Laboratory

DISTRIBUTION

Internal

DIR
Dr. von Braun

R-DIR
Mr. Weidner

R-AERO
Dr. Geissler

R-ASTR
Dr. Haeussermann

R-COMP
Dr. Hoelzer

R-FP
Mr. Baker

R-ME
Dr. Kuers

R-P&VE
Dr. Mrazek
Mr. Wegrich (-PT)

R-QUAL
Dr. Grau

R-TEST
Mr. Heimburg

R-RP
Dr. Stuhlinger
Mr. Heller
Mr. Bucher
Mr. Cannon
Mr. Mathis
Mr. Downey
Dr. Shelton
Dr. Dozier
Mr. Miles
Dr. Mechtly
Mr. Arnett
Mr. Atkins
Mr. Bannister (25)
Mr. Fields
Mr. Fletcher
Mr. Fountain
Mr. Gates
Mr. Harrison
Mr. Jones
Dr. Lal
Mr. Merrill
Mr. Miller
Dr. Schocken
Mr. Snoddy
Mr. vun Kannon
Mr. Watkins
Mr. Weathers
Mr. Holland (-P)
Reserve (15)

IO
Dr. Johnson
Miss Smith
Mr. Faulkner
Mr. Arrendale
Mr. Cade

MS-IPL (8)

MS-IP

MS-IS (6)

MS-H

HME-P

CC-P

MS-T (5)

DISTRIBUTION (Concluded)

External

OSSA Headquarters
National Aeronautics and Space Administration
Washington, D. C. 20546
Attn: Mr. M. A. Edwards
Code SL

OART Headquarters
National Aeronautics and Space Administration
Washington, D. C. 20546
Attn: Mr. Conrad Mook (3)
Code RV-1

Fairchild-Hiller Corporation
Rockville, Maryland
Attn: Mr. Robert Eby (3)

Illinois Institute of Technology
Chicago, Illinois
Attn: Mr. Gene Zerlaut

National Research Corporation
70 Memorial Drive
Cambridge 42, Massachusetts
Attn: Mr. Jack Light

Jet Propulsion Laboratory
4800 Oak Grove Drive
Pasadena, California 91103
Attn: Mr. Joseph Plamondon
Mr. Donald Lewis

Ames Research Center
Moffett Field, California 94035
Attn: Mr. C. B. Neel
Mr. E. R. Streed

Goddard Space Flignt Center
Greenbelt, Maryland
Attn: Mr. Robert Kidwell

Manned Spacecraft Center
Houston, Texas 77058
Attn: Mr. Walter Guy

Scientific and Technical Information
Facility (25)
Attn: NASA Representative (S-AK RKT)
P. O. Box 5700
Bethesda, Maryland